Title:

Mechanistic within-host models of the asexual *Plasmodium falciparum* infection: a review and analytical assessment

Authors:

Flavia Camponovo[1,2,3], Tamsin E. Lee[1,2], Jonathan Russell[4], Lydia Burgert[1,2], Jaline Gerardin[4], Melissa A. Penny[1,2*]

[1] Swiss Tropical and Public Health Institute, Basel, Switzerland

[2] University of Basel, Basel, Switzerland

[3] current address: Center for Communicable Disease Dynamics, Department of Epidemiology, Harvard T. H. Chan School of Public Health, Boston, MA 02115, USA

[4] Institute of Disease Modeling, Bill & Melinda Gates Foundation, 500 5th Ave N, Seattle, WA 98109, USA

[5] Northwestern University, Chicago, USA

[*] corresponding author

Keywords

Plasmodium falciparum, within-host mathematical models, asexual parasite dynamics

Abstract

Background: Malaria blood-stage infection length and intensity are important drivers of disease and transmission; however, the underlying mechanisms of parasite growth and the host's immune response during infection remain largely unknown. Over the last 30 years, several mechanistic mathematical models of malaria parasite within-host dynamics have been published and used in malaria transmission models.

Methods: We identified mechanistic within-host models of parasite dynamics through a review of published literature. For a subset of these, we reproduced model code and compared descriptive statistics between the models using fitted data. Through simulation and model analysis, we compare and discuss key features of the models, including assumptions on growth, immune response components, variant switching mechanisms, and inter-individual variability.

Results: The assessed within-host malaria models generally replicate infection dynamics in malaria-naïve individuals. However, there are substantial differences between the model dynamics after disease onset, and models do not always reproduce late infection parasitemia data used for calibration of the within host infections. Models have attempted to capture the considerable variability in parasite dynamics between individuals by including stochastic parasite multiplication rates; variant switching dynamics leading to immune escape; variable effects of the host immune responses; or via probabilistic events. For models that capture realistic length of infections, model representations of innate immunity explain early peaks in infection density that cause clinical symptoms, and model representations of antibody immune responses control the length of infection. Models differed in their assumptions concerning variant switching dynamics, reflecting uncertainty in the underlying mechanisms of variant switching revealed by recent clinical data during early infection. Overall, given the scarce availability of the biological evidence there is limited support for complex models.

Conclusions: Our study suggests that much of the inter-individual variability observed in clinical malaria infections has traditionally been attributed in models to random variability, rather than mechanistic disease dynamics. Thus, we propose that newly developed models should assume simple immune dynamics that minimally capture mechanistic understandings and avoid over-parameterisation and large stochasticity which inaccurately represent unknown disease mechanisms.

Background

The complex life cycle of *Plasmodium falciparum* (*P. falciparum*) involves many parasite stages within both the mosquito and human host. *P. falciparum* induces complex and non-sterilizing immune responses with repeated possible exposure in both the human host and mosquito. The human blood-stage infection plays a crucial role in both disease burden and transmission. Indeed, the length and magnitude of asexual parasite infection both drive clinical symptoms within a host and the transmission potential through the level of gametocytes. Thus, understanding within-host dynamics of the asexual parasite stage is essential for both the development of drugs or other tools that target asexual or gametocytes stages, and to assess burden or transmission dynamics. Within a human host, the *P. falciparum* malaria cycle begins with sporozoites transmitted by infectious mosquito bites that travel from the skin to the liver (1). Following replication in the liver, merozoites are released into the bloodstream (1,2). These merozoites subsequently infect red-blood cells (RBCs) and *in vitro,* approximately 16 merozoites emerge from a single merozoite in a 48 hour asexual blood-stage cycle (3). The blood-stage infection can persist for over 300 days if untreated (4). A small fraction of asexual parasites convert into gametocytes (2), responsible for the transmission from human to mosquito.

The asexual malaria life cycle drives clinical disease in an individual, with many processes eliciting or evading the immune response (1). After invasion of a RBC, merozoites are no longer directly exposed to immune actors. However, with hundreds of parasite proteins exported to the erythrocyte's cell surface, immune effectors can recognize an infected RBC (iRBC) (1). Naturally acquired immune responses recognize erythrocyte surface antigens of iRBCs or antigens of the free merozoites (1), as well as antigens from liver and sexual stages (5,6). Exported parasite proteins on the cell's surface give the cell the capability to adhere to the blood vessel's wall, and thus evade splenic clearance (1). Furthermore, expression of the most characterized exported protein, the erythrocyte membrane protein 1 (PfEMP1), can be switched by the parasites from a large library of variants (1). New protein conformations are produced to avoid detection, requiring the host to mount new immune responses (1). *P. falciparum* escapes the immune response by successively expressing one out of 50–60 different PfEMP1 genes (7). The switching mechanisms remain uncertain, but switching between the PfEMP1 variants needs to be quick enough to evade the immune system and avoid splenic

clearance, while slow enough to avoid variant exhaustion and maintain the chronic nature of the infection (7). In endemic areas where populations are continuously exposed to malaria, repeated infections lead to acquired immunity, preventing severe cases of malaria and death but without leading to sterilizing protection for infection (1).

Many mathematical and statistical models have been developed to understand population level dynamics of malaria transmission and impact of interventions (reviewed in (8,9)), or to understand within host dynamics. Although there is a long history of mathematical modeling of malaria parasite within-host dynamics over the years, the substantial biological unknown elements of both parasite and host dynamics and the highly variable nature of infection patterns, make it difficult to assess model accuracy. Furthermore, as there is limited within-host data available for infections from either immunologically naïve or non-naïve individuals, there is no "gold standard" data set or model to compare. In 1999 Molineaux and Dietz reviewed published intra-host models (10), indicating the first within-host model of malaria was likely developed in 1989 by Anderson et al. (11). Anderson and colleagues (11) described parasite dynamics via a set of differential equations representing uninfected RBCs, iRBCs, merozoites, and immune effectors (11). This model along with the others reviewed led Molineaux and Dietz to conclude that existing models lacked realism and did not make quantitative comparisons to real data. They further concluded that the reviewed models did not allow for inter-individual variability in the outputs, even though a large variation in infection dynamics exists between individuals (10). In part to address these concerns, a substantial number of mechanistic within-host models, either standalone or used in larger transmission models, have since been developed. Most of these models were initially parameterized to data from naïve patients, but not necessarily to the limited available data from previously exposed individuals.

Several sources of detailed observations of parasite dynamics and densities in naïve patients exist. In the past, malaria infection was induced to generate fever to treat other illnesses. In particular between 1917–1963 malaria was used as a therapy to treat patients with tertiary neurosyphilis before the use of penicillin (12). The most extensive malaria therapy data set was collated between 1940 and 1963 by Collins and Jeffery (12–15). The published database consists of 318 patients treated at Columbia, South Carolina and the Milledgeville, Georgia laboratories (12). This data, referred to here as the malariatherapy dataset, includes patients infected with three different strains of *P. falciparum* for neurosyphilis treatment. The data

113 captures daily parasite counts by microscopy of both gametocyte and asexual parasites, and
114 daily fever charts are available for each patient. This data set is the only detailed
115 representation of the entire *P. falciparum* infection in a naïve population. Other malaria
116 therapy data sets exist, for example of *P. vivax* infection in naïve and non-naïve individuals
117 (16) (not further discussed here).

118 Over the last decade, many individual-based models of malaria transmission dynamics have
119 been developed (reviewed in (8)); several of these include models of within-host asexual
120 parasite dynamics (17–20). A recently published paper (21) investigated common biological
121 assumptions made by within-host models, and concluded that current knowledge is
122 insufficient to capture infection lengths and to explain the chronic nature of malaria
123 infections. They further concluded their model was quite sensitive to small changes in the
124 parameters leading to large instabilities in estimated infection lengths (21). Since asexual
125 parasite dynamics are particularly important for modelling the effect of malaria interventions
126 targeting humans (such as drugs or vaccines), the within-host model assumptions in these
127 models have the potential to drive predictions at the population level, on either disease
128 burden or intervention impact. Thus, with these within host models widely used in public
129 health research, a good understanding of the overall dynamics, the assumptions, the
130 uncertainties, and limitations of the models are key to critically assess and understand the
131 predictions arising from the use of those models.

132 In this review, we analyzed within-host models of asexual parasitemia, and identified which
133 components of the models drive predicted dynamics. We identified models used to
134 investigate malaria interventions such as drugs or vaccines, either as stand-alone within-host
135 models or used in combination with transmission models. The review and analytical
136 assessment of each model, including the re-simulation of a subset of models to allow for
137 deeper investigation, provides an overview of the main components of each model and their
138 underlying assumptions. Rather than defining a gold standard, we discuss how models differ
139 in their immune responses and parasite growth. Our comparison provides an understanding of
140 the benefits and limitations in using these models, which directs and informs future work on
141 within-host models of blood-stage parasitemia.

142

143 Methods

144 Models and simulation code:

145 We identified several mechanistic within-host models currently implemented in individual-
146 based models (IBMs) from a recently published systematic review of IBMs (8), or used as
147 stand-alone models to understand within host dynamics or assess malaria interventions (drugs
148 or vaccines) targeting humans. The within-host models identified as being part of malaria
149 IBMs are Molineaux *et al.* (22), Johnston *et al.* (23), Gatton and Cheng (24), Eckhoff (19),
150 McKenzie and Bossert (25), and Gurarie *et al.* (26). We additionally included the models of
151 Childs and Buckee (21) and Challenger (27) (see Fig. 1, and further details on the models in
152 *Results* and in the Additional file 1). Five of the eight identified models were re-simulated for
153 a deeper understanding of the underlying dynamics.

154 For the simulations, we used the open access code of Johnston *et al.* (23) to recreate the
155 Johnston *et al.* model in Matlab (28). As both Johnston *et al.* (23) and later model Challenger
156 *et al.* (27) were based on the model of Molineaux *et al.* (22), the code of Johnston *et al.* was
157 used as base code to reproduce the Molineaux *et al.* (22) and the Challenger *et al.* (27)
158 models. Challenger *et al.* provides open access code for their model in C++ (29) which we
159 used to validate our model code. The model of Gatton and Cheng. (24) was not open access
160 but we reproduced the model in Matlab. The model code for Eckhoff (19) was available from
161 the author's affiliated groups (30).

162 Model simulation and assessment:

163 Each model was simulated 1750 times, which for the patient-specific model of Molineaux *et*
164 *al.* corresponds to 50 simulations of the 35 malaria therapy patients used for
165 parameterization. For all other models, this corresponds to 1750 independent realizations of
166 the stochastic models.

167 Parameter values were fixed to the values defined in their respective publication (note that
168 the parameters are either assumed from literature or fitted in their models, Additional file 1
169 Table S3). The same stochastic multiplication rate of each PfEMP1 variants was used in the
170 models of Molineaux *et al.* and Johnston *et al.*, except that for Johnston *et al* any
171 multiplication rate over 35 was resampled to be within the ranges defined by their model, as

172 defined in their publication. Other models either had a different definition of the parasite's
173 multiplication rates (Challenger *et al.*) or a constant multiplication rate (Gatton and Cheng,
174 and Eckhoff). Except for Eckhoff, our model simulations were undertaken in Matlab (28).
175 The Eckhoff model was simulated in C++ (30). All subsequent analysis of results was
176 performed in R (31). For the purpose of comparison, the models are all simulated for 600
177 days. Furthermore, we did not select for the best fit of the model to each patient and did not
178 add measurement errors (as done by *Molineaux et al.*), as the aim was not to replicate the data
179 but to illustrate the internal behavior of the models.

180 We initially assessed models via nine summary statistics for the malariatherapy data set.
181 These summary statistics were first described in Molineaux *et al.* (22), and were later used as
182 evaluation measures for several of the other models (23,24,27). Briefly, the nine summary
183 statistics computed are *i)* the slope of the linear regression line from the first positive
184 observed parasitemia to the first local maximum; *ii)* the $\log_{10}$ parasite density of the first local
185 maximum, with a local maximum defined as a parasite density greater than the three
186 preceding time steps (t-1 to t-3) and not lower than the three following time steps (t+1 to
187 t+3); *iii)* the number of local maxima; *iv)* the slope of the linear regression through all the
188 $\log_{10}$ local maxima; *v-vi)* the geometric mean and standard deviation of the geometric means
189 between the local maxima; *vii-viii)* the proportion of positive observation in the first half and
190 second half of the interval between the first and last positive observation; and *ix)* the last
191 positive day (22). A positive parasite density observation was defined as an asexual parasite
192 density equal to, or higher than, 10 iRBC per microliter. In the Gatton and Cheng model the
193 number of iRBCs is modeled, and thus for consistency and for comparison to other models,
194 the output was converted to iRBC per microliter assuming a body contains five liters of blood
195 (24).

196 <u>Assessment of parasite growth and host immunity for the re-simulated models</u>

197 In addition to the summary statistics, we compared estimated overall parasite multiplication
198 rates, the innate, variant specific, general adaptive, and total immune responses, and the
199 subsequent variation across the simulations that reflects individual variation and stochasticity.
200 We compared models by visual inspection of time series plots of these response components
201 and established the model's main drivers of parasite density and infection length predictions.

To assess the modeled parasite growth, for the models which use a stochastic and variant-specific multiplication rate, we defined an average inherent parasite multiplication rate (across variants) at each time-step for each model. In Molineaux *et al.* and Johnston *et al.* each variant-specific parasite has its own multiplication rate drawn from a Normal distribution (22,23). Therefore, the average multiplication rate of all parasites at each time step is the weighted average of the variant-specific parasite multiplication rates, as follows:

$$\bar{M}(t) = \frac{\sum_{i=1}^{i=50} m_i p_i(t)}{P_{tot}(t)}, \qquad \textit{eq. 1}$$

where m_i is the multiplication rate of variant *i*, $p_i(t)$ the parasite density of variant *i* at time *t*, and $P_{tot}(t)$ the total parasite density at time *t*. For all other models, the overall parasite multiplication is an input parameter and thus does not need to be calculated.

To investigate the modeled immune responses, we categorized immune responses into innate (S_c), variant-specific (S_v), and general adaptive (S_m). Between Molineaux *et al.*, Johnston *et al.,* and Challenger *et al.,* those three terms are directly comparable across models, but for Gatton and Cheng and Eckhoff the terms are slightly different (see Additional file 1 Table S2). Where the variant specific immune response is tracked for each variant (in Molineaux *et al.,* Johnston *et al.* and Gatton and Cheng), the overall effect of the variant-specific immune response is the weighted average of the variant-specific immune response, as follows:

$$\overline{S_v}(t) = \frac{\sum_{i=1}^{i=50} S_{v,i}(t) p_i(t)}{P_{tot}(t)}, \qquad \textit{eq. 2}$$

where $S_{v,i}(t)$ is the effect of the immune response on variant *i* at time *t*, $p_i(t)$ the parasite density of variant *i* at time *t*, and $P_{tot}(t)$ the total parasite density at time *t*. The innate and general adaptive immune responses are described as an effect on the total parasite density and are reported as such without further modifications. All equations and comparison between the models are summarized in Additional file 1 Table S2.

Results

Overall model structure:

Via the systematic review of IBMs (8), six mechanistic within-host models were identified as part of the transmission models, as represented in Fig. 1, namely Molineaux *et al.* (22), Gatton and Cheng (24), Johnston *et al.* (23), Eckhoff (19), McKenzie and Bossert (25), and Gurarie *et al.* (26). An additional two models were identified through further literature search, namely Challenger *et al.* (27), and Childs and Buckee (21). The new quantitative results in the current study focus on five models, namely those of Molineaux *et al.* (22), Gatton and Cheng (24), Johnston *et al.* (23), Challenger *et al.* (27), and Eckhoff (19) (Fig. 1). The models of McKenzie and Bossert (25), Gurarie *et al.* (26), and Childs and Buckee (21) were included in the summary categorizations for comparison.

Most models reviewed here can generally be described in a simple discrete form

$$Y_t = m_t Y_{t-1} R_t \ .$$

Here parasite densities or number of parasites Y_t, at time t, depend on the parasite's multiplication rate m_t reduced by the effect of immune response R_t. The immune response R can represent up to four components: the innate immune response, and the antibody-driven immune response defined by variant specific, cross-reactive, and adaptive immune responses, each component including different levels of stochasticity and different functions. The models can be relatively simple and reproduce a smoothed time-course of an infection, such as in McKenzie and Bossert, or include a higher level of complexity to describe more granular parasite dynamics including the typical peaks and throughs observed in clinical data. The latter usually involves explicit or implicit inclusion of a range of variant-specific parasites.

We reviewed each model via their detailed descriptions and equations in their respective publications. The models are fully described in the Additional file 1 and their main characteristics are described in Table 1, with more details of their immune response dynamics summarized in Table 2. We classified the type of equations used, the level of stochasticity integrated into the models, and detailed which dataset/s were used for calibration. We further categorized key features of parasite growth and immune dynamics for each model and

255 summarized in tables (Table 1 and Table 2). Equations were classified and divided into four
256 descriptions 1) parasite growth defined by the merozoite multiplication factor; 2a) triggering
257 of, and effect of, the innate immune response; 2b) PfEMP1 variant-specific immunity
258 dynamics; and 2c) the general or non-PfEMP1 immune response dynamic. Fig. 2 illustrates
259 the simplified dynamics and feedback between the host and parasite for the different models.
260 The description of the parasite growth in each model is described in Table 1 (row "Assumed
261 multiplication rate") and the immune responses are described in Table 2. The complete
262 description of each model is given in Additional file 1, and a brief summary is provided here.

263 Model specificities:

264 Molineaux *et al.* describe a mechanistic malaria parasite growth model including three
265 components of the immune response, namely an innate immune response acting early in the
266 infection; a variant-specific immune response for each variant-specific parasite population;
267 and a general adaptive immune response acting on total parasite population. This model was
268 intended to reproduce parasite densities from patients in the malariatherapy dataset (12), and
269 describes each of the 50 variant-specific parasite populations within an infection. The model
270 of Molineaux *et al.* was adapted by Johnston *et al.* by replacing two patient-specific
271 parameters which trigger innate and general adaptive immune response with values drawn
272 from a distribution (see Additional file 1). Challenger *et al.* further simplified the model by
273 tracking total parasite density instead of 50 variant-specific parasite densities to reduce
274 memory and computational requirements. The Johnston *et al.* and Challenger *et al.* models
275 are referred to as *Molineaux adapted* models in this manuscript.

276 At a similar time to the publication of Molineaux *et al.*, Paget-McNicol *et al.* (32) published a
277 stochastic model also including three immune response components and exploring different
278 assumptions on switching dynamics of the PfEMP1 variant expression. This model was later
279 adapted by Gatton and Cheng (24). Instead of a set of discrete model equations with
280 stochastic parameters describing the asexual parasite density in the blood as in Molineaux *et*
281 *al*, the Gatton and Cheng model is stochastic and represent the total number of asexual
282 parasites as a decision tree, where parasite numbers trigger choice of path in this decision tree
283 and corresponding model equations (24). This model differs significantly from Molineaux *et*
284 *al.* in regard to assumptions around the variant switching dynamics. Additionally, Gatton and
285 Cheng include cross-reactivity between variant-specific immune responses, which was not

286 present in the model of Molineaux *et al,* although the general adaptive immune response
287 might capture the effect of cross-reactivity implicitly.

288 More recently, two additional models by Eckhoff (19) and by Childs and Buckee (21) were
289 developed. Eckhoff's model represents both continuous events such as immune responses to
290 iRBC and discrete events such as the bursting of schizont and the associated immune
291 responses. It also includes the concept of immune memory, capturing faster immune
292 responses when an individual is re-exposed to a previously seen parasite variant.
293 Additionally, it includes cross-reactivity between variant-specific antibody responses. In the
294 early infection days, the probability of switching to a new variant increases with growing
295 parasite population. The model developed by Childs and Buckee (21) is deterministic and in
296 their work they explored a wide parameter space to assess variations in the infection
297 dynamics with parameter choice. This model includes four different immune responses,
298 namely innate; variant-specific; general adaptive immune responses; and similarly to the
299 models of Eckhoff and Gatton and Cheng, includes cross-reactive immune response across
300 parasite variants. Childs and Buckee investigate different variant switching dynamics, and
301 explicitly limit parasite growth by available RBCs and competition of immune cells for each
302 variant-specific immune response.

303 Despite these models incorporating detailed variant switching, the malariatherapy calibration
304 datasets contain no information on gene expression profiles. Thus, there is no data describing
305 variant expression and variant switching dynamics in the included patients. Instead, the
306 models utilized understandings from the literature at the time of model development on
307 potential structured switching; some of the models emphasize and discuss the uncertainty
308 around the switching assumptions. Molineaux *et al.* and Johnston *et al* assume that immune
309 pressure drives the switch to the expression of a new variant, based on biological studies with *P.*
310 *knowlesi* infections in monkeys (7). In contrast, Paget-McNicol *et al.* refute the theory that
311 switching depends on immunity because it can also be observed *in vitro* (33), and Gatton and
312 Cheng's modified model also assumes no link between variant switching mechanisms and
313 host immune pressure. To avoid all variants being expressed with equal chances, the models
314 either assume different switching probabilities for each variant according to a geometric
315 distribution (as in Molineaux *et al*, and in Johnston *el al*), limit the number of available
316 variants to switch to in each cycle (as in Eckoff), or assume two groups of variants, with either
317 fast or slow switching behavior hypothesized at the time in (34) (as in Gatton and Cheng). The

model in Childs and Buckee explores different switching networks where all variants can switch to all other variants but with different probabilities and favoring some variants over others (which was adapted from (35)).

The two last models in this review, Gurarie *et al.* and McKenzie and Bossert, are simpler models which do not include variant switching and variant-specific immune responses: thus, including only two immune response components. Gurarie *et al*. propose a discrete model that assumes the effect of the adaptive immune response is forced to have "random falls" which implicitly allow for the immune response to lose effectivity when the parasite switches to a new variant. These falls in immune response decrease in magnitude during the course of an infection, as it is assumed that the general adaptive immune response builds up. The model of McKenzie and Bossert is the only model presented here which is built around a set of differential equations in a continuous time frame. Although capable of representing the general infection pattern (high initial peak followed by a decrease in parasitemia), the model is less granular, causing model predictions to resemble a smoothed version of the malariatherapy time-series data. This model was developed to allow for different genotypes to infect the host, and to explore the effect of different gametocyte dynamics on malaria transmission. This model does not include variants nor allow for variant switching dynamics to impact immune dynamics.

<u>Including inter-individual variability:</u>

The models attempt to replicate time-series observed in subsets of the malariatherapy data, either with formal or less formal fitting, or at least attempting to reproduce the general pattern observed. The Molineaux *et al.* model was fitted to 35 (out of 334) patients from the malariatherapy data, who were spontaneously cured and received no other treatment. Other models used a larger number of malariatherapy patients (Table 1) to be less restrictive and avoid selection biases. More details on model fitting can be found in Additional file 1 Table S3. There is considerable variation in infection dynamics across the malariatherapy patients, both in magnitude and structure of peaks of parasite numbers, and in length of infections (Fig. 3-4). This inter-individual variability inherently includes detection and clinical measurement error but is also a result of the stochastic nature of the biological mechanisms involved. These dynamics and observed variability are challenging to replicate. In order to capture the variability, models often implement stochasticity either in the parameters defining parasite multiplication rate and/or in the implementation and effect of the innate and general

350 adaptive immune responses (Molineaux *et al* and *Molineaux adapted*); by creating a
351 stochastic model with most variables defined by Binomial or Normal distributions (Gatton
352 and Cheng, and Eckhoff); or by fitting parameters separately to each patient (Molineaux *et al*,
353 Mckenzie and Bossert, and Gurarie *et al*). Similarly, the model developed by Childs and
354 Buckee is deterministic but can include different infection patterns by varying parameter
355 values within the ranges specified in the publication (21).

356 Time series of parasite density

357 Time series of parasite density, summary statistics (described in *methods*) of true parasitemia
358 profiles from 35 malariatherapy patients (12), alongside time series and summary statistics
359 calculated from 1750 simulated parasitemia profiles for the five models, are shown in Fig. 3
360 and 4, and in Additional file 1 Table S1. We further note that although care was taken with
361 new or adapted code, there may be small differences from the original publications.

362 The observed $\log_{10}$ parasite densities of the 35 patients from the malariatherapy data varies
363 significantly across the patients, a variability which appears to be accounted for in the models
364 (Fig. 3). In Molineaux *et al.* most infections cease before day 200, with a subset of simulated
365 parasitemia appearing to be chronic infections that do not end before the end of the
366 simulation. The model of Johnston *et al.* increased the variant-specific immune response
367 decay compared to Molineaux *et al.*, thereby decreasing the immune response's efficiency.
368 This results in increased simulated infection lengths compared to the simulations in
369 Molineaux *et al.* The general shape of decay in parasite densities from Johnston *et al.* also
370 appears to be more exponential-like compared to the other models, which is most likely a
371 result of the more significant effect of the general adaptive immune response. In Challenger
372 *et al.,* simulations indicate a general pattern of two peaks, the first is followed by a decrease
373 as a result of the innate immune responses, followed by a second wave of parasitemia that is
374 controlled by the variant-specific and general immune responses. Simulations from Gatton
375 and Cheng indicate a slightly different time course of peaks compared to those predicted
376 from Molineaux *et al.* and the models adapted from Molineaux *et al*. Simulations from
377 Gatton and Cheng indicate a general first peak with a sharp decrease in parasite densities with
378 initial innate immune responses, followed by new peaks in parasite densities given the
379 probabilistic approach taken in Gatton and Cheng (see Additional file 1 Table S2 for the
380 equations). The general decline in predicted parasite densities (decreasing peaks) is not
381 reflected in the summary statistics (Fig. 4). In Eckhoff's model the first peak is followed by

382 much lower peaks, resulting in a steeper slope of peaks in the summary statistics (Fig. 4). The
383 average infection lengths are consistent with the 35 malariatherapy dataset, although it is
384 worth noting that the Eckhoff model was fitted to a larger dataset from the malariatherapy
385 patients including more than the 35 patients in Molineaux *et al*.

386 Total parasite multiplication rate during infection

387 We tracked each variant-specific parasite density in our simulations in all models except
388 Challenger *et al.* and Eckhoff, the former because the equations do not explicitly model each
389 variant and the latter due to the computational complexities of tracking each variant. The
390 average multiplication rate at each time step is shown in Fig. 5. For Gatton and Cheng and for
391 Eckhoff*,* the multiplication rate of the parasites, defined as the multiplication rate without the
392 effect of any host immune response, is fixed at 16 per cycle and remains the same for all
393 simulations and time (Fig.4d-e). For Johnston *et al.* and Molineaux *et al.,* each variant-
394 specific parasite has its own multiplication rate drawn from a Normal distribution with mean
395 of 16. For each time step, the overall multiplication rate for Johnston *et al.* and Molineaux *et*
396 *al.* is thus the weighted average of the variant-specific multiplication (see *methods).*
397 Therefore, these two models have a constant multiplication rate, in time, for each variant-
398 specific parasite. However, the overall multiplication rate fluctuates over time, representing
399 the competition between variant-specific parasites (with different multiplication factors), with
400 new variants appearing, and other variants disappearing throughout the infection. For some
401 simulations (Molineaux *et al.* and Johnston *et al.*), the overall multiplication rate is high at
402 the beginning of the infection (Fig. 5a-b) and causes a peak in parasitemia density. The
403 predicted infection length for a subset of simulations from both Molineaux *et al.* and
404 Johnston *et al.* is very long, and in these subsets of simulations, the overall multiplication rate
405 is in fact high throughout the infection (see Additional file Fig. S2).

406 In Challenger *et al.*, the multiplication rate at each time step is an input parameter of the
407 model. It is both drawn from a Normal distribution with mean 16 and correlates with the
408 previous time step (27) (see Additional file 1 Table S2). Thus, the median multiplication rate
409 across all simulations remains constant at 16 by design (Fig. 5c). Taking the example of a
410 single simulation (Fig. 6), the pattern of overall parasitemia in the Challenger model is less
411 driven by the average growth rate in time compared with the simulations for Molineaux *et al.*
412 and Johnston *et al.* (Fig. 6a-c). Molineaux *et al.* reported that a varying overall parasite
413 multiplication rate, and thus the parasite inherent proliferation rate (without immunity), is

414 essential to recreate observed peaks in parasitemia in the dataset. Furthermore, we note that
415 long lasting infections can only occur in models that express highly multiplying variants.
416 Overall, this indicates infection dynamics in Molineaux *et al.* and Johnston *et al.* are
417 primarily driven by stochasticity in the inherent growth of the parasites, whereas in
418 Challenger *et al.,* Gatton and Cheng, and Eckhoff, the stochasticity in their predicted
419 dynamics is driven more by immune responses and subsequent killing effects.

420 Immune response dynamics in the models

421 In terms of immune response variability between the simulations (and thus assumed to exist
422 between individuals), the highest variance across individuals arises from the variant-specific
423 immune response, followed by the innate immune response, with the general adaptive
424 response being reasonably consistent across individuals for the models (Fig. 5-6). The key
425 assumptions around immune dynamics for each model are summarized in Table 2. The
426 simulated immune responses are shown for four models in the first plots in Fig. 5, and
427 examples of single simulations are shown in Fig.5. Note that in Gatton and Cheng and in
428 Eckhoff, the effects of the immune responses are drawn from Binomial distributions; thus,
429 the variability in the effects of the immune responses are not entirely captured in the immune
430 time plots of Fig. 3 and Fig. 5.

431 The innate immune response is mainly active at the beginning of the infection (approximately
432 the first 20-50 days in the different models) as it responds directly to high levels of parasite
433 density. In Eckhoff's model, the innate immune response is modulated by the adaptive
434 immune response, reducing with increasing antibodies against the parasite population,
435 making this model the only one with direct feedback between innate and adaptive immune
436 response.

437 The variant specific immune response, effective against variant-specific parasite after delay,
438 is modeled for each variant explicitly in Molineaux *et al.*, Johnston *et al.*, Gatton and Cheng,
439 and Eckhoff. The increased decay rate in Johnston *et al.* compared to Molineaux *et al.* leads
440 to a reduction in the immune responses (Fig. 5). In Challenger *et al.*, once the variant-specific
441 immune response is activated, it is quickly efficient in reducing parasite densities compared
442 to the other two models (steeper slope in the variant-specific immune response curve in Fig.
443 5). This efficient immune response likely explains the steep decrease after the first wave of
444 parasite density. In Gatton and Cheng, the variant-specific response is activated when the

variant-specific parasite density reaches the threshold of 12 PRBC/μl (24), and the magnitude is increased if the antibody was already produced during the infection. When there are high peaks throughout the infection, the variant-specific immune response remains very active throughout the predicted infections from Gatton and Cheng.

The general adaptive immune response increases in time since the start of the infection, responding to the cumulative parasite density (Molineaux *et al., Molineaux adapted,* Eckhoff, McKenzie and Bossert, and Gurarie *et al.* model), time (Gatton and Cheng) or a combination of both time and parasite density (Childs and Buckee). An important finding is that by comparing all three immune responses and the total net immune response (Fig. 5 and 6), the general immune response is the main effector of reducing parasite density in all models approximately after 50 days from start of infection. However, the variant immune response will ultimately end the infection. The decrease of the critical density for the general adaptive immune response in Johnston *et al.* and Challenger *et al.* compared to Molineaux *et al.* (see model description and Table S2 in Additional file 1) leads to a higher effect of the general adaptive immune response in those models, which compensates for the weaker effect of the variant-specific immune response.

Discussion

In this study, we have reviewed eight published mechanistic within-host models of the asexual blood-stage dynamics of *P. falciparum*, of which we reproduced five. We compared predicted time-series of asexual parasitemia, modelled growth rates, innate immune responses, variant-specific immune responses, and general adaptive immune responses. The models varied widely in complexity. Whilst rather simple models such as McKenzie and Bossert have the advantage that they do not rely heavily on assumptions of unknown biological mechanisms, they reproduce less detailed patterns of infection. In contrast, more complex models such as Eckhoff or Childs and Buckee capture more detailed immune mechanisms but also include more uncertainty. Understanding the variation in multiplication rates, versus immune responses, or random effects and measurement error, and their impact on parasite density variations is particularly important when the models are included in broader investigations of the effect of a vaccine, drug or other

473 interventions aimed to modify parasite growth patterns. The overview presented here provides
474 a general understanding of those models.
475
476 Model composition varies in complexity and uncertainty

477 Parasite and host dynamics are represented in the mechanistic models via detailed description
478 of the parasite replication dynamics, and up to four host immune responses. Each model has
479 its own additional complexity, specifications, and advantages. For example, to obtain
480 increased detail of the host's response, some models include red blood cell availability and
481 limit the maximum immune response capacity. Or, to include more details in the parasite
482 dynamics, some models include specific variant switching mechanisms. Models generally
483 define a negative feedback loop between the parasite density or cumulative parasite density
484 since the start of the infection and the effect of the immune responses, and in addition some
485 models add the time of infection (Gatton and Cheng, Childs and Buckee, Eckhoff) as a
486 determinant for the magnitude of the general immune response.

487 Including stochasticity in the models is particularly relevant for the within host dynamics of *P.*
488 *falciparum* as the infection patterns observed in the malariatherapy data are highly variable
489 among patients. Our analysis highlighted that the Molineaux *et al.* and the *Molineaux adapted*
490 models have likely allocated too much stochasticity to the individual parasite multiplication
491 rates, thus masking other mechanisms and placing relatively less importance on immune
492 responses. Furthermore, for these models, we found their assumptions concerning the
493 inherent multiplication rates of the parasites differ from other models, along with
494 assumptions of large variability in the variant-specific parasite multiplication rates in the
495 absence of any immune response. These dynamics were found to be essential in the Molineaux
496 *et al.* and *Molineaux adapted* models to reproduce clinical malaria therapy patterns of infection,
497 rather than immune responses (22). In particular, in Molineaux *et al.* and Johnston *et al.,* longer
498 infections result from the expression of variants with a high multiplication rate towards the end
499 of the infections for later variants. In contrast, the other models did not rely on variation to
500 capture infection patterns. Instead, variation was mainly included in the control of infection
501 due to immune responses and switching mechanisms.

502 For models including multiple parasite variants, the variant switching dynamics are an
503 important mechanism driving the parasitemia predictions. The switching dynamics define
504 how the parasite goes from expressing one PfEMP1 variant to another one at the next

505 generation in order to evade the immune response. Switching dynamics in the models have
506 been assumed to respond to the variant specific immune response (Molineaux *et al.* and
507 Johnston *et al.*), to the current variant population size (Eckhoff), or were determined by more
508 sophisticated switching networks (Childs and Buckee, Gatton and Cheng). In the re-simulated
509 models, the variant-specific immune response, which is driven by the parasite's variant
510 switching dynamics either explicitly, or implicitly in Challenger *et al.*, was the most variable
511 component of the immune responses across individuals. This is in contrast to the data available
512 to inform switching dynamics over the course of an infection, which is limited to early days of
513 infection (36–38).

514 The various assumptions around the mechanisms of action of the different immune responses
515 and the interplay between parasite and host highlight the challenge of realistically
516 reproducing the time-series observed in the malariatherapy dataset, especially the inter-
517 individual variability. This challenge is confounded since there is limited knowledge of the
518 biological mechanisms at play.

519 <u>Parasite multiplication rates might be lower than initially assumed</u>

520 It is commonly agreed that a single iRBC produces 16 merozoites (3), of which a portion
521 successfully invade new erythrocytes. Growth rates *in vivo* are more difficult to measure, and
522 compared to the assumed multiplication factor of 16, includes the host-parasite interactions
523 which reduce the observed parasite growth. Several independent statistical models previously
524 estimated parasite growth at onset of infections in both malaria therapy or volunteer infection
525 studies (VIS). Estimates from the malariatherapy dataset range between 10-18 (39), or 6-24
526 (20). In malaria VIS the growth factor was estimated to be between 12-15 (40), and in the
527 control cohort of vaccines AMA1-based vaccine challenge between 14-21 (41). More recently,
528 estimated *ex-vivo* multiplication factors for different malaria genotypes were found to be
529 between 2-11 for laboratory strains and new clinical isolates (42). One hypothesis explaining the
530 variation among parasite growth relies on the differential capacity of the PfEMP1-variants to
531 evade splenic clearance, with the hypothesis that a subgroup of PfEMP1 expressing parasites
532 might be fast growing (due to increased cytoadherence and thus decreased splenic clearance)
533 (43). This mechanism may explain differing growth rates among parasites expressing different
534 variants, and explain apparent higher multiplication rates in naïve individuals if their parasites
535 express the fast growing PfEMP1 subgroup (43). Variance in parasite multiplication rates
536 among clones and among infections across individuals is possible due to this variance in

537 successful avoidance of splenic clearance during blood-stage replication, however, it is
538 unclear whether the range should include an overall multiplication factor as large as 32 or 35, as
539 in some models reviewed here (namely in (21–23,27)).

540 Variant switching and immune response modeling are limited by current knowledge

541 Switching mechanisms are not well understood, and it remains unclear if the switching
542 mechanisms are driven by antibody response (as in [1], [2]) or are not directly influenced by the
543 immune pressure (as in (21,24)). In contrast to the assumptions made in the models reviewed
544 here, it is likely that parasites express more than one variant, if not all variants, during the first
545 blood stage generation. As highlighted by Childs and Buckee (21), this finding challenges the
546 current understanding on the underlying mechanisms leading to chronic infections. The concept
547 of cross-reactivity, suggested as a mechanism necessary for chronic infections (44) and included
548 explicitly in Gatton and Cheng, Childs and Buckee, and in Eckhoff would not be applicable, as
549 modeled and explored by Childs and Buckee, if the majority of the variants are expressed at the
550 onset of asexual parasitemia (45). The lack of understanding about the switching dynamics
551 supports the assumptions in Challenger *et al.*, as they only model total parasitemia without
552 modeling switching between variants. The models described by McKenzie and Bossert, and
553 Gurarie *et al.*, are less complex and do not model variant-specific parasitemia, offering potential
554 modeling alternatives when detailed mechanisms of immune response are not needed. To our
555 knowledge, there are few biological studies on the kinetics and interplay of the immune
556 responses as defined by the models (innate, variant specific, and/or adaptive immune
557 response). As such it is unclear how much each immune component affects the overall time
558 course of infection. Therefore, it is not surprising that models differ in the relative importance
559 of general or variant-specific immune responses. Moreover, in the absence of a clear
560 biological understanding of the variability in infection time-series, model stochasticity remains
561 an important driver of the modelled immune and parasite dynamics.

562 Further data for new models

563 It is essential to highlight here that the malariatherapy dataset cannot be considered as a
564 typical time course of an infection, as the data come from patients with severe neurosyphilis,
565 who were malaria naïve, and did not include children. Furthermore, inoculations were limited
566 a restricted set of parasite strains. Thus, although the malariatherapy data are the only
567 detailed data available on infection time-course, models are not strictly evaluated by their

568 ability to reproduce malariatherapy-like infections. Data on early infections are available in
569 high detail from VIS. They provide precise quantification of parasitemia at much lower
570 detection threshold than the malariatherapy data, and variant expression dynamics or other
571 genetic traits relevant for understanding the dynamics in the first few days of blood stage
572 infection can now be informed by such studies. Beyond early infections, models need to rely
573 on longitudinal field data to assess their performance. Longitudinal field data are extremely
574 important to explore the dynamics in realistic settings, with individuals living in endemic
575 areas who are repeatedly exposed to malaria, including children who are most at risk for the
576 disease, and including a range of genetic diversity and complexity of infection. Because
577 immunity builds up with age and exposure (46), and genetic diversity is a result of immune
578 pressure, longitudinal and cross sectional field studies which include genetic analysis give
579 important insights in malaria infection dynamics.

580 The current analysis and review focused on infections in naïve individuals and we did not
581 review the models for their ability to capture infections in pre-exposed individuals. Although
582 data is lacking, the immune effect of pre-exposure could be added to the models as a second
583 step, for example by adding an overall reduction factor that would lower the magnitude of the
584 parasite density in function of age and/or exposure, similar to an empirical model by Maire *et*
585 *al.* (47). The effect of co-infection was not included here and its implementation was a focus
586 of the Childs and Buckee model (21), which hypothesizes that co-infections and super-
587 infections have different effects based on the timing of the second infection, and that the
588 effects of multiple infections seem to be poorly understood, and thus poorly included in
589 models (21). Recently many field studies focusing of genetic data and analysis are giving
590 insights in the effect and dynamics of multiple infections on a population scale (for example
591 (48,49)), yet empirical data on the time course of complex infections are sparse and
592 insufficient to validate models of co-infections, relying on data from mouse models for
593 detailed infection dynamics (50,51).

594 Conclusions

595 This review provides insights on existing models of asexual *P. falciparum* blood-stage
596 infections, and some insights on both known and unknown biological mechanisms driving
597 infection dynamics. Blood-stage parasite densities are at the core of malaria transmission,

598 morbidity and mortality. Thus, population models that include models of within-host parasite
599 dynamics to estimate the impact of blood-stage drugs or vaccine, or estimate the impact of
600 parasite resistance, should be aware of the underlying assumptions made in the within-host
601 model and how those changes effect infection dynamics. As in any modeling exercise, the
602 choice of the model and its degree of complexity should depend on the specific biological,
603 epidemiological, or public health question, and should account for available data.

List of abbreviations

(i)RBC: (infected) red blood cell
P. falciparum : Plasmodium falciparum
PfEMP1: Plasmodium falciparum erythrocyte membrane protein 1
VIS : Volunteer infection studies

Declarations

Ethics approval and consent to participate
Not applicable

Consent for publication
Not applicable

Availability of data and materials
The outputs generated and analyzed during the current study are available from the corresponding author on reasonable request

Competing interests
The authors declare that they have no competing interests

Funding

The design, analysis, and writing of the manuscript was funded by the Swiss National Science Foundation through the SNF Professorship of MAP: PP00P3_170702

Authors' contributions

Conception: FC, MAP - Design: FC, MAP - Analysis: FC, MAP, JR and JG - Interpretation: FC, MAP, TEL, LB, JR, JG - Drafted the work: FC - Substantial revision: FC, MAP, TEL, LB. All authors have reviewed and approved the manuscript

Acknowledgements

We acknowledge and thank our colleagues in the Infectious Disease Modeling unit of the Swiss Tropical and Public Health Institute for fruitful discussions that led to improvement of this work. We thank Lauren Childs for discussions on her model in particular as well as for the other models.

Figures and Tables

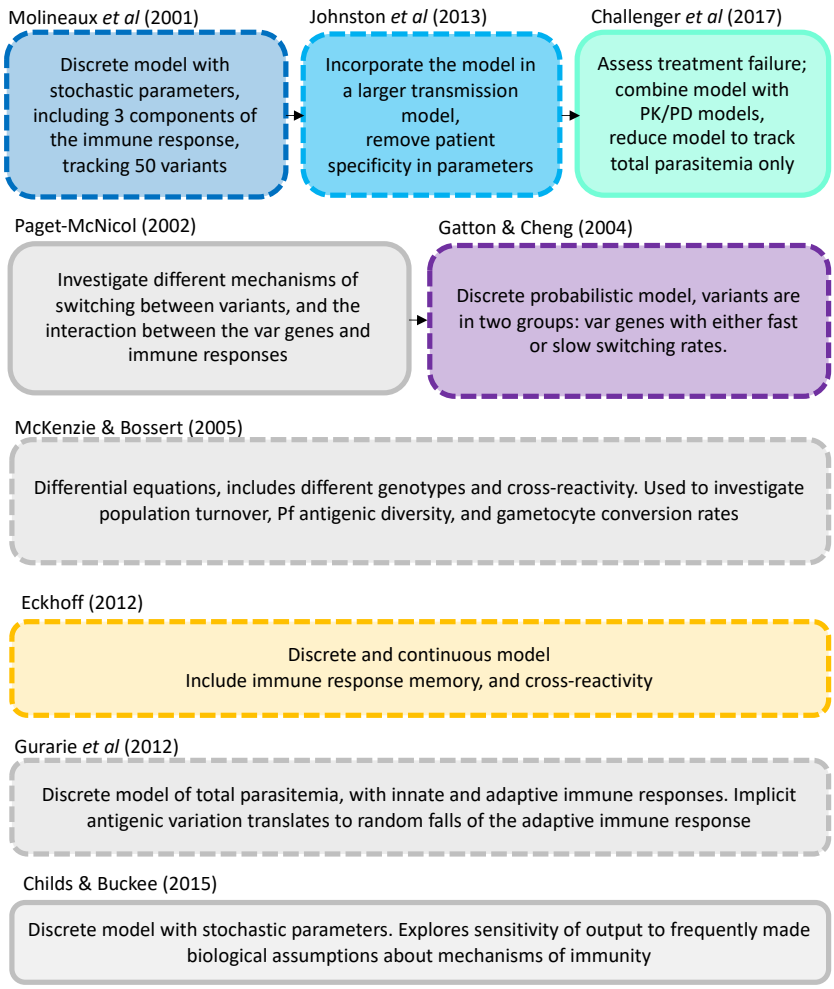

Figure 1: Identified within-host models of asexual parasite blood stage infection. *Models are ordered by their publication date on the vertical and horizontal axis, with models adapted from another model displayed on the same row and linked with arrows. Dashed squares represent models that have been used in IBMs according to the systematic review of [6], and colored squares highlight the models that are simulated in this study, where the colors correspond to the results plotted in Fig. 3-6. Text in each box indicates a brief description of the main features or differences of the models. A more detailed description of the models can be found in the supplementary material or in the source publications (17–19,21,22,24,27)*

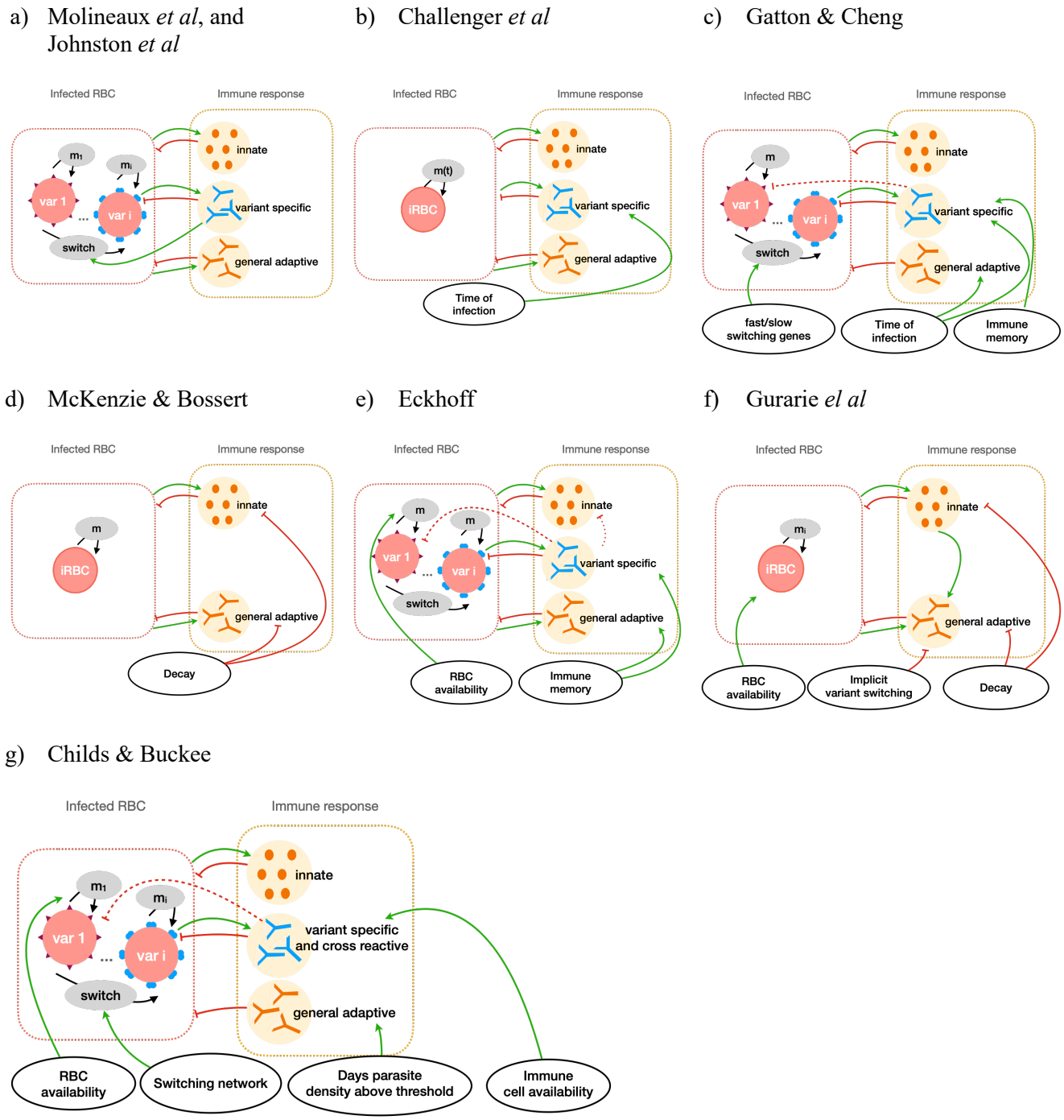

Figure 2: Schematic overview of the main within host dynamics. *A simplified representation of the main immune and parasite dynamics for a) Molineaux et al. and Johnston et al., b) Challenger et al., c) Gatton et al, d) Mckenzie and Bossert, e) Eckhoff, f) Gurarie et al., and g) Childs and Buckee. Each model is represented by the main parasite components (left box), the host-immune component (right box) and additional factors influencing parasite dynamics (bottom circles). Models either describe overall infected red blood cells (iRBC) or total iRBC result from a sum of variant specific iRBC (var*

1,..,i).Asexual multiplication (m) and variant switching of the parasite are represented by black arrows, and feedbacks between parasite and host components are represented by green arrows or red bar-headed lines for positive or negative effects, respectively. The weaker effect due to cross-reactive immune response is represented by dashed bar-headed lines. A more detailed description of the models can be found in the supplementary material, or in the source publications (17–19,21,22,24,27)

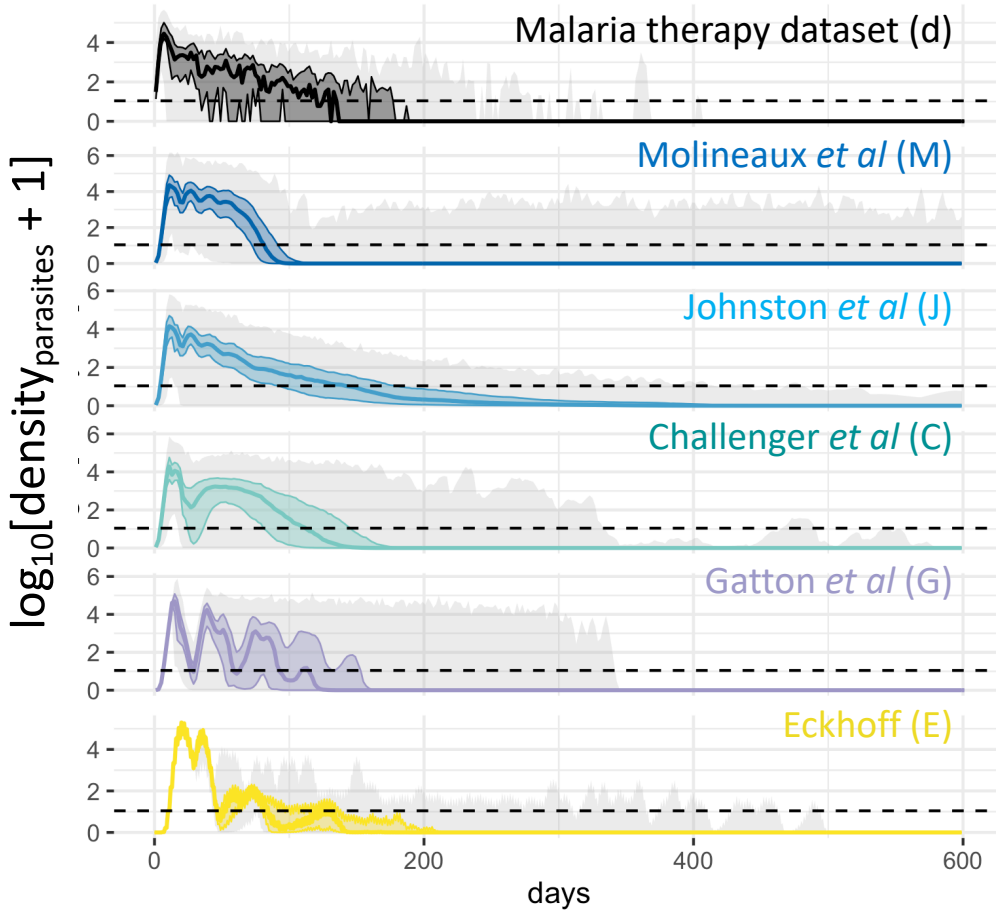

662

663 ***Figure 3: Observed and predicted total asexual parasite density.*** *From top to bottom, the*
664 *observed* $\log_{10}$ *asexual parasite density in time of the 35 patients from the malaria therapy*
665 *dataset (d), and the predicted* $\log_{10}$ *asexual parasite density in time from the Molineaux et al.*
666 *(M), the Johnston et al. (J), the Challenger et al. (C), the Gatton & Cheng. (G), and the*
667 *Eckhoff simulations (E). The solid line represents the median across the 1750 simulations per*
668 *model or 35 patients for the dataset, the colored shaded area the interquartile range (Q25-*
669 *Q75) and the light grey shaded area the minimum and maximum. The horizontal dashed line*
670 *indicated the threshold of positive observation (10PRBC/µl)*

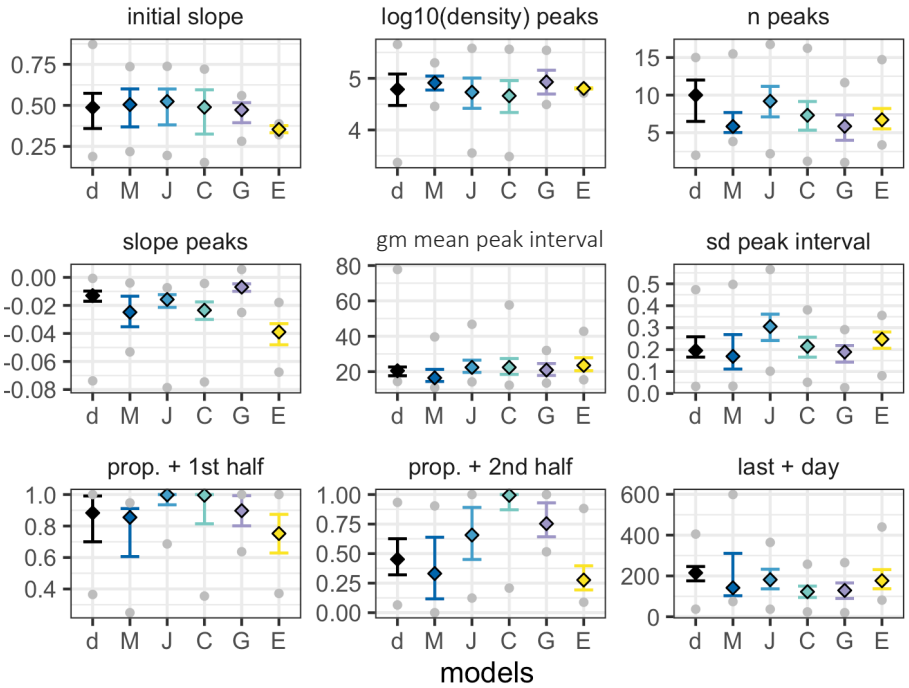

Figure 4: Descriptive summary statistics of the observed and predicted time course of total asexual parasite density. *The nine descriptive summary statistics as defined in Molineaux et al. (see methods), for the dataset and the 5 models (by color). Squares indicate the median, bars the interquartile range and the grey dots the minimum and maximum. In each plot, from left to right, the estimates are shown for the 35 patients from the malaria therapy dataset (d), and for the simulated models of Molineaux et al. (M), Johnston et al. (J), Challenger et al. (C), Gatton & Cheng. (G), and Eckhoff (E).*

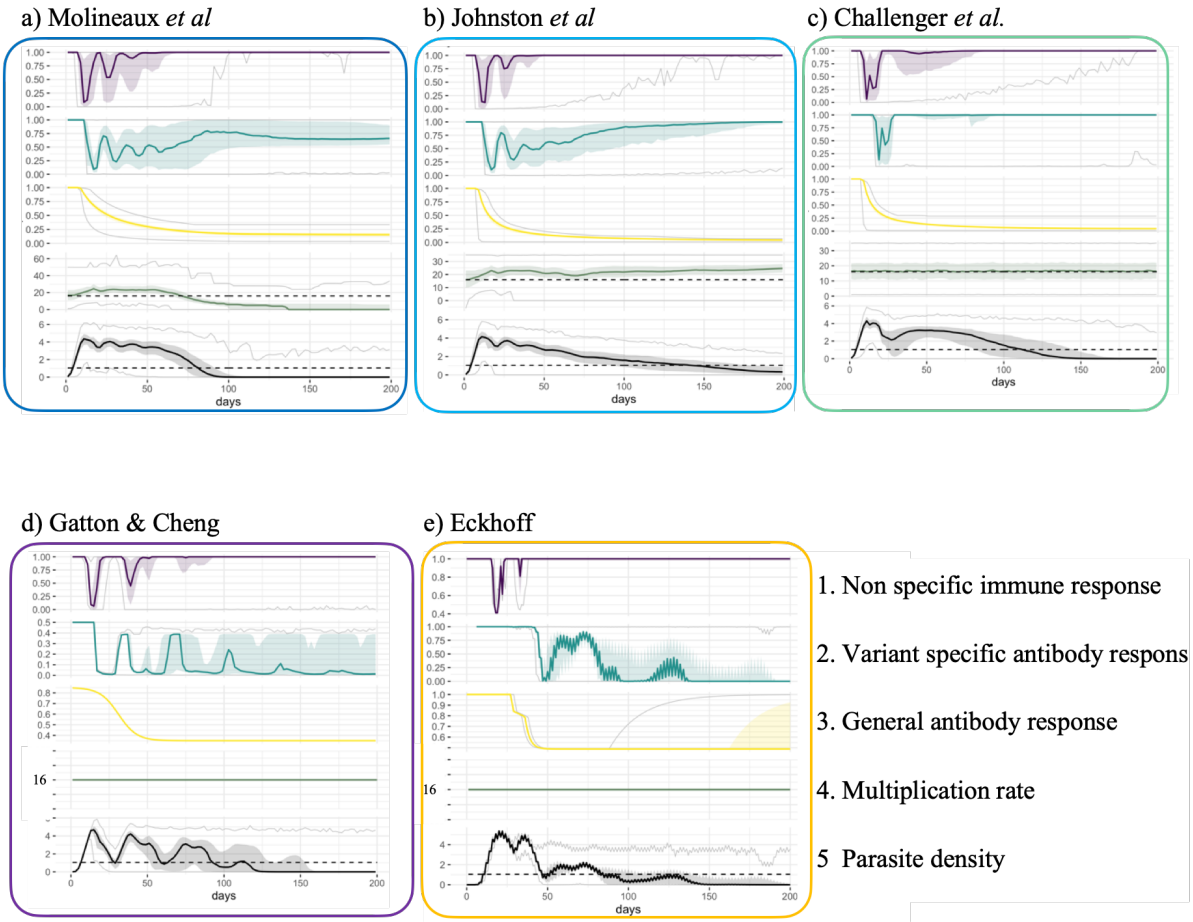

Figure 5: Immune responses, multiplication rates and asexual parasite densities in different models. *Each panel shows, from top to bottom, 1. the effect of the innate immune response, 2. the effect of the variant specific immune response (see methods for calculations), 3. the effect of the general adaptive immune response, 4. the net effect of the product of the three immune responses, 5. the average (across variants, see methods) multiplication rate, 6. the* $\log_{10}$ *asexual density and 7. the product of the overall multiplication rate with the net effect of the immune response. The x-axis represents days of infection, the solid line the median, the shaded area the interquartile range (Q25-Q75) and the grey lines the minimum and maximum resulting from the 1750 simulations. The horizontal dashed green line represents an overall multiplication rate of 16, the horizontal dashed black line indicates the threshold of positive density (10PBRC/µl). Results are shown for* ***a)*** *Molineaux et al.,* ***b)*** *Johnston et al., and* ***c)*** *Challenger et al.,* ***d)*** *Gatton & Cheng, and* ***e)*** *Eckhoff.*

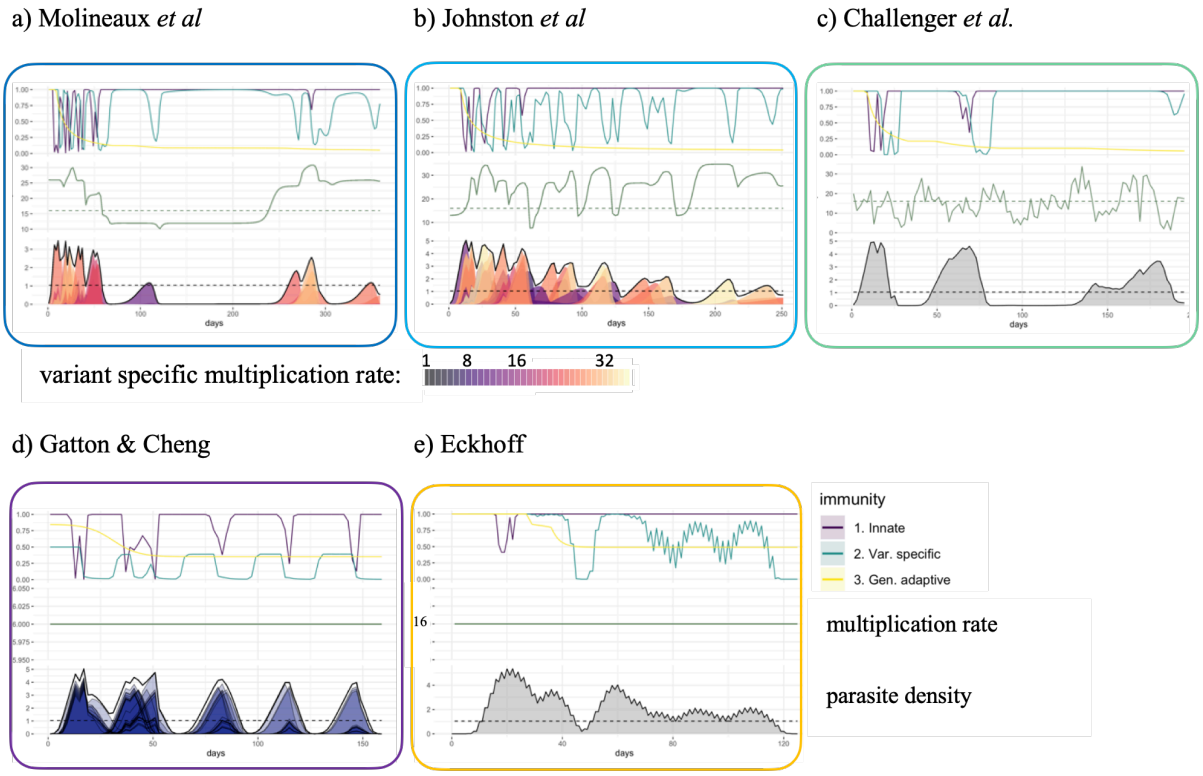

Figure 6: Example of the immune responses, multiplication rates and asexual parasite densities in single simulations from several models. *Each panel shows, from top to bottom, 1-3. the effect of the innate, variant specific (see methods for calculations), and general adaptive immune responses; 4. the net effect of the product of the three immune responses; 5. the overall (across variants, see methods) multiplication rate; 6. the* $\log_{10}$ *asexual density and variant specific asexual parasite density; and 7. the product of the overall multiplication rate with the net effect of the immune response. The x-axis represents days of infection. The horizontal dashed green line represents an overall multiplication rate of 16, the horizontal dashed black line indicates the threshold of positive density (10 PBRC/μl). Results are shown for* ***a)*** *Molineaux et al.,* ***b)****. Johnston et al.,* ***c)*** *Challenger et a.l,* ***d)*** *Gatton & Cheng, and* ***e)*** *Eckhoff.*

707 ***Table 1: Overview and main description of the models.*** *The model description includes the main characteristics of variant or total parasite*
708 *growth, the stochastic components, and the data used for fitting.*

General model structure, and parasite dynamics								
Models	**Molineaux *et al.***			**Gatton & Cheng**	**Eckhoff**	**Childs & Buckee**	**Gurarie *et al.***	**McKenzie & Bossert**
Adapted models		**Johnston *et al.***	**Challenger *et al.***					
Publication year	2001	2013	2017	2004	2012	2015	2012	2005
Discrete (2 days time step) or continuous	Discrete			Discrete	Mixed	Discrete	Discrete	Continuous
Patient specific parameters	Yes*	No		No	No	No	Yes**	Yes***
Tracks all parasite variants	Yes	Yes	No	Yes	Yes	Yes	No	No
Number of variants at the start of infection	1		-	5	5	5	-	-
Main assumption on variant switching dynamics	Dependent on variant immune response. Different switching probability for each variant follows geometric distribution		-	Fast and slow switching variants. Independent of immune response, described in (52)	Switching rate per iRBC, thus larger population have higher probability to introduce new variant. Parasites can switch to 7 available variants, out of a total of 50 variants, in each round.	Different switching networks are investigated. Network assumed from (35)	Not explicit	-

Assumed multiplication rates	different for every variant but constant in time ($\sim\mathcal{N}(\mu_m = 16, \sigma_m = 10.4)$)		(for overall parasites) different for every time step, but correlated to previous time step	16 (const)	16 (const)	variant-dependent but constant in time ($\sim\mathcal{N}(\mu_m = 16, \sigma_m = 8)$)	range between 15-50, median 23.91	-
Additional assumptions on growth	-	-	-	-	dependent on RBC availability	dependent on RBC availability	dependent on RBC availability	-
Variability included in the model: • **stochastic parameters**	multiplication rate, patient specific parameters for the critical densities for innate and general adaptive immune response		critical densities for innate and general adaptive immune response, and growth rate			most parameters chosen stochastically (for sensitivity analysis)	merozoite invasion probability and replication rate, innate and adaptive immune response efficiency and activation threshold, antigenically distinct variant clusters	None
• **probabilistic equations**				effect of immune responses, antibody production, variant switching	variant switching, effect of variant specific and innate immune response		falls of immune response due to antigenic switch taken at random	None
Data used for the fitting[a]	35 patients[1]			90 patients[2]	Malariatherapy data[3]	-[4]	122 malaria therapy patients	63 malaria therapy patients[5]

* Patient specific critical densities for innate and general adaptive immune response calculation.
**** Model calibrated to each of the infection chart separately to generate 50 best parameter sets for each calibrated** malariatherapy **data set.**
***** Model fitted to each of the infection chart separately, thus all parameters take a patient specific value or are averaged across patients.**
[1] *P. falciparum* infections classified as spontaneous cures, out of a total of 334 patients in the malariatherapy data.
[2] Patients from the malariatherapy dataset not treated to modify the primary parasitaemia, and with no curative or subcurative treatment after the primary attack.
[3] Number of patients is not specified. Includes those with high initial peaks and treated during the primary peak.
[4] The model focuses on the effect on outcome of varying the parameters, within biologically reasonable ranges.
[5] inoculated with McLendon. From the patients only the days before any drug or other interventions were used, which included a range between 22 – 159 days of infection.
[a] as described in the initial publications, the models might have been re-fitted when updated, implemented in other research projects, or implemented in transmission models.

710 ***Table 2: Overview and main immune dynamics of the models.*** *The model description includes the main characteristics of innate, variant*
711 *specific, and general adaptive immune response.*

General model structure, and parasite dynamics								
Models	**Molineaux *et al.***	**Johnston *et al.***	**Challenger *et al.***	**Gatton & Cheng**	**Eckhoff**	**Childs & Buckee**	**Gurarie *et al.***	**McKenzie and Bossert**
Adapted models								
Assumptions on innate immune response	dependent on total parasite density at a given time				dependent on density of each parasites expressing variants for which there is no antibody response, and on the rupturing of iRBCs	dependent on total parasite density at a given time and is capped by a maximum efficacy term	dependent on iRBC density	dependent on cumulative asexual parasite density
Assumptions on variant specific immune response	dependent on the variant specific parasite density, and lasting in time with a decaying intensity		dependent on the total parasite within a time frame preceding the time of response, and on time after infection start	Triggered by a variant specific parasite density threshold, dependent on the time after infection start, and the magnitude increases if the antibody has been produced previously	dependent on the variant specific parasite density	dependent on the variant specific parasite density, a maximum growth and decay rate. And is restricted by total number of immune cells available	not explicit, but adaptive immune response includes random falls due to implicit variant switching	-
Assumptions on general adaptive immune response	depends on cumulative total parasite density			dependent on the time after the start of the infection	modeled as immune response against merozoite antigens - increase every 2 days, dependent on parasite density	dependent on cumulative number or days the total parasite population is above 10^7	dependent on iRBC density and combined innate and adaptive effector pool	Dependent on cumulative asexual parasite density, does not decay in time
Includes cross-reactivity	No		Not explicitly	Yes, the variant specific response approximately kills 5% of all other variants	Yes, response to variants randomly assigned to 5 subgroups	Yes, response to variants randomly assigned to subgroups	No	Yes, immune response to one genotype can be activated by the presence of another genotype
Other comments	innate and adaptive immune			parameters differ with different parasite strains	immune memory is included in the model	Detailed sensitivity analysis resulted in		

	response include patient specific parameters					significant impact on the model's outcome of small changes in parameter values, highlighting the challenged face by within host models		

712

713

714 References

715 1. Cowman AF, Healer J, Marapana D, Marsh K. Malaria: Biology and Disease. Cell. 2016
716 Oct;167(3):610–24.

717 2. Miller LH, Ackerman HC, Su X, Wellems TE. Malaria biology and disease pathogenesis:
718 insights for new treatments. Nat Med. 2013 Feb;19(2):156–67.

719 3. Matthews H, Duffy CW, Merrick CJ. Checks and balances? DNA replication and the cell
720 cycle in Plasmodium. Parasit Vectors. 2018 Dec;11(1):216.

721 4. Felger I, Maire M, Bretscher MT, Falk N, Tiaden A, Sama W, et al. The Dynamics of
722 Natural Plasmodium falciparum Infections. Gosling RD, editor. PLoS ONE. 2012 Sep
723 18;7(9):e45542.

724 5. Idris ZM, Chan CW, Kongere J, Hall T, Logedi J, Gitaka J, et al. Naturally acquired
725 antibody response to Plasmodium falciparum describes heterogeneity in transmission on
726 islands in Lake Victoria. Sci Rep. 2017 Aug 22;7(1):9123.

727 6. Ouédraogo AL, Roeffen W, Luty AJF, de Vlas SJ, Nebie I, Ilboudo-Sanogo E, et al.
728 Naturally Acquired Immune Responses to Plasmodium falciparum Sexual Stage
729 Antigens Pfs48/45 and Pfs230 in an Area of Seasonal Transmission ▿. Infect Immun.
730 2011 Dec;79(12):4957–64.

731 7. Kyes SA, Kraemer SM, Smith JD. Antigenic Variation in *Plasmodium falciparum* : Gene
732 Organization and Regulation of the *var* Multigene Family. Eukaryot Cell. 2007
733 Sep;6(9):1511–20.

734 8. Smith NR, Trauer JM, Gambhir M, Richards JS, Maude RJ, Keith JM, et al. Agent-based
735 models of malaria transmission: a systematic review. Malar J [Internet]. 2018 Dec [cited
736 2019 Mar 31];17(1). Available from:
737 https://malariajournal.biomedcentral.com/articles/10.1186/s12936-018-2442-y

738 9. Mandal S, Sarkar RR, Sinha S. Mathematical models of malaria - a review. Malar J. 2011
739 Jul 21;10:202.

740 10. Molineaux L, Dietz K. Review of intro-host models of malaria. Parassitologia.
741 1999;41:221–31.

742 11. Anderson RM, May RM, Gupta S. Non-linear phenomena in host—parasite interactions.
743 Parasitology. 1989 Jan;99(S1):S59.

744 12. Collins WE, Jeffery GM. A Retrospective Examination of Sporozoite- and Trophozoite-
745 Induced Infections with Plasmodium Falciparum: Development of Parasitologic and
746 Clinical Immunity during Primary Infection. Am J Trop Med Hyg. 1999 Jul
747 1;61(1_Supplement):4–19.

13. Collins WE, Jeffery GM. A retrospective examination of mosquito infection on humans infected with Plasmodium falciparum. Am J Trop Med Hyg. 2003 Mar 1;68(3):366–71.

14. Collins WE, Jeffery GM. A retrospective examination of sporozoite-induced and trophozoite-induced infections with Plasmodium ovale: development of parasitologic and clinical immunity during primary infection. Am J Trop Med Hyg. 2002 May 1;66(5):492–502.

15. Collins WE, Jeffery GM. A Retrospective Examination of the Patterns of Recrudescence in Patients Infected with Plasmodium Falciparum. Am J Trop Med Hyg. 1999 Jul 1;61(1_Supplement):44–8.

16. Roberts JM, Jeffery GM, Collins WE. A retrospective examination of reinfection of humans with Plasmodium vivax. Am J Trop Med Hyg. 2004 Jun 1;70(6):642–4.

17. Gurarie D, Karl S, Zimmerman PA, King CH, St. Pierre TG, Davis TME. Mathematical Modeling of Malaria Infection with Innate and Adaptive Immunity in Individuals and Agent-Based Communities. Paul RE, editor. PLoS ONE. 2012 Mar 28;7(3):e34040.

18. McKenzie FE, Bossert WH. An integrated model of Plasmodium falciparum dynamics. J Theor Biol. 2005 Feb;232(3):411–26.

19. Eckhoff P. P. falciparum Infection Durations and Infectiousness Are Shaped by Antigenic Variation and Innate and Adaptive Host Immunity in a Mathematical Model. Snounou G, editor. PLoS ONE. 2012 Sep 19;7(9):e44950.

20. Dietz K, Molineaux L, Raddatz G. Mathematical model of the first wave of Plasmodium falciparum asexual parasitemia in non-immune and vaccinated individuals. Am J Trop Med Hyg. 2006 Aug 1;75(2_suppl):46–55.

21. Childs LM, Buckee CO. Dissecting the determinants of malaria chronicity: why within-host models struggle to reproduce infection dynamics. J R Soc Interface. 2015 Feb 11;12(104):20141379–20141379.

22. Molineaux L, Diebner HH, Eichner M, Collins WE, Jeffery GM, Dietz K. Plasmodium falciparum parasitaemia described by a new mathematical model. Parasitology [Internet]. 2001 Apr [cited 2019 Mar 21];122(04). Available from: http://www.journals.cambridge.org/abstract_S0031182001007533

23. Johnston GL, Smith DL, Fidock DA. Malaria's Missing Number: Calculating the Human Component of R0 by a Within-Host Mechanistic Model of Plasmodium falciparum Infection and Transmission. Antia R, editor. PLoS Comput Biol. 2013 Apr 18;9(4):e1003025.

24. Gatton ML, Cheng Q. Investigating antigenic variation and other parasite host interactions in Plasmodium falciparum infections in nave hosts. Parasitology. 2004 Apr;128(4):367–76.

25. McKenzie FE, Bossert WH. An integrated model of Plasmodium falciparum dynamics. J Theor Biol. 2005 Feb;232(3):411–26.

26. Gurarie D, Karl S, Zimmerman PA, King CH, St. Pierre TG, Davis TME. Mathematical Modeling of Malaria Infection with Innate and Adaptive Immunity in Individuals and Agent-Based Communities. Paul RE, editor. PLoS ONE. 2012 Mar 28;7(3):e34040.

27. Challenger JD, Bruxvoort K, Ghani AC, Okell LC. Assessing the impact of imperfect adherence to artemether-lumefantrine on malaria treatment outcomes using within-host modelling. Nat Commun [Internet]. 2017 Dec [cited 2019 Mar 21];8(1). Available from: http://www.nature.com/articles/s41467-017-01352-3

28. MATLAB and Statistics Toolbox Release 2018b, The MathWorks, Inc., Natick, Massachusetts, United States.

29. Challenger J. JDChallenger/adherence_project [Internet]. 2017 [cited 2019 Apr 25]. Available from: https://github.com/JDChallenger/adherence_project

30. Bershteyn A, Gerardin J, Bridenbecker D, Lorton CW, Bloedow J, Baker RS, et al. Implementation and applications of EMOD, an individual-based multi-disease modeling platform. Pathog Dis [Internet]. 2018 Jul 1 [cited 2020 Dec 25];76(5). Available from: https://academic.oup.com/femspd/article/doi/10.1093/femspd/fty059/5050059

31. R Development Core Team (2008). R: A language and environment for statistical computing. R Foundation for Statistical Computing, Vienna, Austria. ISBN 3-900051-07-0, URL http://www.R-project.org.

32. Paget-Mcnicol S, Gatton M, Hastings I, Saul A. The Plasmodium falciparum var gene switching rate, switching mechanism and patterns of parasite recrudescence described by mathematical modelling. Parasitology [Internet]. 2002 Mar [cited 2019 Mar 21];124(03). Available from: http://www.journals.cambridge.org/abstract_S0031182001001160

33. Peters J, Fowler E, Gatton M, Chen N, Saul A, Cheng Q. High diversity and rapid changeover of expressed var genes during the acute phase of Plasmodium falciparum infections in human volunteers. Proc Natl Acad Sci. 2002 Aug 6;99(16):10689–94.

34. Bull PC, Berriman M, Kyes S, Quail MA, Hall N, Kortok MM, et al. Plasmodium falciparum Variant Surface Antigen Expression Patterns during Malaria. PLoS Pathog. 2005;1(3):e26.

35. Noble R, Christodoulou Z, Kyes S, Pinches R, Newbold CI, Recker M. The antigenic switching network of Plasmodium falciparum and its implications for the immuno-epidemiology of malaria. Pascual M, editor. eLife. 2013 Sep 17;2:e01074.

36. Wang CW, Hermsen CC, Sauerwein RW, Arnot DE, Theander TG, Lavstsen T. The Plasmodium falciparum var gene transcription strategy at the onset of blood stage infection in a human volunteer. Parasitol Int. 2009 Dec;58(4):478–80.

37. Bachmann A, Petter M, Krumkamp R, Esen M, Held J, Scholz JAM, et al. Mosquito Passage Dramatically Changes var Gene Expression in Controlled Human Plasmodium falciparum Infections. Dzikowski R, editor. PLOS Pathog. 2016 Apr 12;12(4):e1005538.

38. Lavstsen T, Magistrado P, Hermsen CC, Salanti A, Jensen AT, Sauerwein R, et al. Expression of Plasmodium falciparum erythrocyte membrane protein 1 in experimentally infected humans. Malar J. 2005 Apr 27;4:21.

39. Simpson JA, Aarons L, Collins WE, Jeffery GM, White NJ. Population dynamics of untreated Plasmodium falciparum malaria within the adult human host during the expansion phase of the infection. Parasitology [Internet]. 2002 Mar [cited 2019 Mar 25];124(03). Available from: http://www.journals.cambridge.org/abstract_S0031182001001202

40. Cheng Q, Gregor L, Stowers A, Lisa R-C, Alison C, Richard C, et al. Measurement of Plasmodium Falciparum growth rates in vivo: a test of malaria vaccines. Am J Trop Med Hyg. 1997;495–500.

41. Duncan CJA, Sheehy SH, Ewer KJ, Douglas AD, Collins KA, Halstead FD, et al. Impact on Malaria Parasite Multiplication Rates in Infected Volunteers of the Protein-in-Adjuvant Vaccine AMA1-C1/Alhydrogel+CPG 7909. Gregson A, editor. PLoS ONE. 2011 Jul 22;6(7):e22271.

42. Murray L, Stewart LB, Tarr SJ, Ahouidi AD, Diakite M, Amambua-Ngwa A, et al. Multiplication rate variation in the human malaria parasite Plasmodium falciparum. Sci Rep [Internet]. 2017 Dec [cited 2019 Mar 26];7(1). Available from: http://www.nature.com/articles/s41598-017-06295-9

43. Abdi AI, Hodgson SH, Muthui MK, Kivisi CA, Kamuyu G, Kimani D, et al. Plasmodium falciparum malaria parasite var gene expression is modified by host antibodies: longitudinal evidence from controlled infections of Kenyan adults with varying natural exposure. BMC Infect Dis [Internet]. 2017 Dec [cited 2019 Mar 31];17(1). Available from: http://bmcinfectdis.biomedcentral.com/articles/10.1186/s12879-017-2686-0

44. Recker M, Nee S, Bull PC, Kinyanjui S, Marsh K, Newbold C, et al. Transient cross-reactive immune responses can orchestrate antigenic variation in malaria. Nature. 2004 Jun;429(6991):555–8.

45. Klein EY, Graham AL, Llinás M, Levin S. Cross-Reactive Immune Responses as Primary Drivers of Malaria Chronicity. Adams JH, editor. Infect Immun. 2014 Jan;82(1):140–51.

46. Rodriguez-Barraquer I, Arinaitwe E, Jagannathan P, Kamya MR, Rosenthal PJ, Rek J, et al. Quantification of anti-parasite and anti- disease immunity to malaria as a function of age and exposure. :20.

47. Maire N, Molineaux L, Smith T, Owusu-Agyei S, Ross A, Dietz K. A model for natural immunity to asexual blood stages of Plasmodium falciparum malaria endemic areas. Am J Trop Med Hyg. 2006 Aug 1;75(2_suppl):19–31.

48. Nkhoma SC, Trevino SG, Gorena KM, Nair S, Khoswe S, Jett C, et al. Co-transmission of Related Malaria Parasite Lineages Shapes Within-Host Parasite Diversity. Cell Host Microbe. 2020 Jan;27(1):93-103.e4.

49. Early AM, Lievens M, MacInnis BL, Ockenhouse CF, Volkman SK, Adjei S, et al. Host-mediated selection impacts the diversity of Plasmodium falciparum antigens within infections. Nat Commun. 2018 Dec;9(1):1381.

50. Bushman M, Antia R, Udhayakumar V, de Roode JC. Within-host competition can delay evolution of drug resistance in malaria. Riley S, editor. PLOS Biol. 2018 Aug 21;16(8):e2005712.

51. de Roode JC, Helinski MEH, Anwar MA, Read AF. Dynamics of Multiple Infection and Within-Host Competition in Genetically Diverse Malaria Infections. :12.

52. Gatton ML, Peters JM, Fowler EV, Cheng Q. Switching rates of Plasmodium falciparum var genes: faster than we thought? Trends Parasitol. 2003 May;19(5):202–8.

Additional file

Mechanistic within-host models of the asexual *Plasmodium falciparum* infection: a review and analytical assessment

Authors:

Flavia Camponovo[1,2,3], Tamsin E. Lee[1,2], Jonathan Russell[4], Lydia Burgert[1,2], Jaline Gerardin[4], Melissa A. Penny[1,2*]

[1] Swiss Tropical and Public Health Institute, Basel, Switzerland

[2] University of Basel, Basel, Switzerland

[3] current address: Center for Communicable Disease Dynamics, Department of Epidemiology, Harvard T. H. Chan School of Public Health, Boston, MA 02115, USA

[4] Institute of Disease Modeling, Bill & Melinda Gates Foundation, 500 5th Ave N, Seattle, WA 98109, USA

[5] Northwestern University, Chicago, USA

[*] corresponding author

Summary of each model

Molineaux *et al. (1)*: The model was developed to reproduce spontaneously cured malaria infection observed in 35 patients of the malariatherapy dataset who were not treated throughout the course of the therapy. The primary aim of the model was to incorporate realistic host immune responses and parasite dynamics, and to eventually include the model in a population transmission model at a later date.

The model described by Molineaux *et al.* is the first model in which immune responses against infection were divided into three components, *i)* the innate immune response, *ii)* the variant specific immune response and *iii)* the general adaptive immune response (variant transcending) (for details see Table S2). It is a discrete model with a 2-day time step to align with the merozoite's 48 hour replication cycle, and the model allows for up to 50 variants of the parasite population. At each time step the observed parasite growth increases as a result of the intrinsic parasite multiplication rate and is reduced by the effect of the three immune responses (with each response ranging between 1 = no effect to 0 = maximum effect). Each infection begins with all 50 variants (denoted by $i = 1,2,\ldots,50$) with initial densities set at 0, except one variant set at 0.1 PBRC/µl. At each time step parasites switch to different variants, with variant specific switching probabilities defined by a constant switching rate. The different probability of switching to each of the variants follows a geometric distribution and is modulated by the variant specific immune responses.

The innate immune response is thought to be triggered early in the infection (first few weeks), and its effect is proportional to the total parasite density at a given time, conditional on a host specific critical density. The variant specific immune response is triggered by the variant specific parasite density, effective after a certain delay (8 days), and persists with a decaying intensity. In addition, the switching mechanisms are controlled by the variant immune response, with the probability to switch to given variant increasing with high total immune responses against each of the 50 variants and decreasing with high immune response against that specific variant. The variant specific immune response, and the capacity of the parasite to switch to new variants, are thought to be a major cause for the different waves of parasitemia, and the chronic pattern of infection. The general adaptive immune response builds up slowly against the conserved part of the parasite, and acts against all variants of the parasite equally. It is effective after a delay (8 days), conditional on a host specific critical

density, and responds to the cumulative parasite density with no decay in time. The general adaptive immune response is assumed to be the main cause of infection clearance, and this is confirmed by simulations except for a few simulations with chronic infection a result of stochasticity in several variant growth rates (see Fig 4 in the main).

In this discrete model, the authors include both patient specific and stochastic parameters to represent the high variability in infection dynamics among the 35 malariatherapy patients (see parameters P_m and P_c, in Table S1). Variant specific parasite multiplication rates are drawn from a Normal distribution with a mean of 16 (truncated at a minimum of 1), leading to different multiplication rates for each of the 50 variants and for each simulation, but constant throughout the infection and different in each simulation. The inter-individual variability is captured by two patient specific parameters representing the critical densities for the innate immune response and the general adaptive immune response. The critical densities are calculated using the first local maximum density, and the length of the infection directly observed for each patient in the dataset.

Molineaux *et al.* additionally added a measurement error and thus were able to reproduce the 35 infections with their model by selecting, as a final step and not included in this analysis, one simulation from a pool of 50 simulations, a pool generated after trial and error, that best fit the min, median, max of the nine summary statistics, using χ^2 test, for each for the 35 patients. This final step makes it difficult to reproduce the authors selection, but general infection dynamics for each patient are possible to reproduce.

Johnston *et al. (2)*: The model was directly adapted from Molineaux *et al.* in order to be included in an individual-based model (IBM), with four parameters re-fitted via bootstrapping method to fit the minmedian and max of the nine summary statistics as well as duration o infection (more details in Table S3). This transmission model was used to understand the human component of the reproductive number R_0, and to investigate the impact of drug treatment (through Pharmacokinetic and Pharmacodynamic (PKPD) models) and drug resistance on transmission (2). To include an adapted Molineaux *et al.* model in a transmission model, they modified the within host model to avoid the two patient specific parameters. Instead, these parameters were drawn from appropriate distributions to maintain inter-individual variability. The authors re-parametrized the patient specific parameters by using the log Normal distribution (for estimates of the first local maximum density) and the Gompertz distribution (for estimates of the length of infection) defined in previously

published literature (3). To maintain the parasite multiplication rates in Johnston *et al.*within a smaller range, and thus a biologically more realistic range compared to Molineaux *et al.*, the Normal distribution was truncated not only at 1, but also on the upper end at 35.

In order to obtain a reasonable fit to the dataset following modification to the critical densities for the innate immune response and the general adaptive immune response, Johnston *et al.* re-fitted three additional parameters. All other parameters were fixed to values from Molineaux *et al*.. The refitted parameters are, *i)* the decay parameter of the acquired variant specific immune response (σ) was increased from 0.02 to 0.15, and *ii)* a constant (k_m) allowing the calculation of the critical density threshold used for the general adaptive immune response (P_m) was reduced from 0.04 to 0.025, and *iii)* a constant (k_c) allowing the calculation of the critical density threshold used for the innate immune response (P_c) was reduced from 0.2 to 0.164. By increasing the decay rate of the acquired variant specific immune response by almost ten-fold, Johnston *et al.* effectively increased infection length as an increased variant specific immunity decay rate (compared to Molineaux *et al.*) leads to a less efficient variant specific immune response. In contrast, parameters k_m and k_c in Johnston *et al.* are coupled to P_m and P_c and potentially increase the strength of the innate and general immune response (see Table S2 for full details).

Challenger *et al. (4)*: Challenger *et al.* adapted the model from Johnston *et al.*, with the aim to assess the impact of treatment adherence and treatment failure (adding PKPD). The main adaptation of Johnston *et al.*, by Challenger *et al.* was reduction of the 50 variant specific parasite densities to a single total parasitemia, thereby reducing the number of equations from 50 to 1, simplifying the model and reducing computational time and memory requirements. The variant specific immune response in Challenger *et al.* is thus a function that represents the response to all variants instead of being the sum of responses to each variant. Early in the infection, the variant specific immune response is modeled similarly to the innate immune responses of Johnston *et al.* and Molineaux *et al.*, except for a different critical density threshold (constant for the innate immune response, stochastic for the variant specific immune response, see Table S2). During the time course of the infection, the variant specific immunity in this model responds not only to the parasite density eight days before (due to assumed delay in activation), but also to earlier time points. Thus Challenger *et al.,* in contrast to Molineaux *et al.* and Johnston *et al.*, implicitly assume immunological memory to

110 previously expressed variants and cross-reactivity *(4)*, despite not tracking all 50 variants (see
111 Fig. S1 and Table S2).

112 Since Challenger *et al.* do not track 50 variants, unlike Molineaux *et al.* and Johnston *et al.*,
113 the model considers an overall multiplication rate across all variants expressed at each time.
114 This overall multiplication rate is computed for each time step, drawn from a Normal
115 distribution around 16 while being positively correlated to the previous time step, implying
116 that this stochastic, but correlated, parasite multiplication rate is the result of the emergence
117 and disappearance of variants during the time course of an infection (4).

118 The model of Challenger *et al.* was fitted to the same 35 malariatherapy patients as in
119 Molineaux *et al.,* fitting the parameters of the overall variant specific immune response and
120 the overall multiplication rate, and re-fitting the constant allowing the calculation of the
121 critical density threshold for the general adaptive immunity (k_m). The authors used Markov
122 chain Monte Carlo method u(Metropolis-Hasting algorithm) to generate random walks in
123 parameter space and fitted the model to the nine summary statistics (see Table S3). A
124 constant that allowed the calculation of the critical density threshold for the general adaptive
125 immunity (k_m) was reduced from 0.0250 to 0.021 which leads to a slightly stronger general
126 adaptive immune response in Challenger *et al.* compared to Molineaux *et al..* Additionally,
127 the critical density threshold of the innate immune response function (P_c) was drawn from a
128 log Normal distribution with $\sigma = 1.2$ instead of $\sigma = 1.148$ as in the other models. All other
129 parameters are identical to the model in Johnston *et al..*

130 **Gatton & Cheng** (5)**:** Gatton & Cheng (5) is a model adapted from a previously published
131 probabilistic model of Paget-McNicol *et al.* (6). The model was fitted to the malariatherapy
132 data differentiated by the *P. falciparum* I strain used. The model was fitted using sets of 100
133 simulations, altering 6 parameters in the model. They compared the model output to four
134 variables, namely maximum parasitemia, number of days with fever, number of days with
135 parasitemia higher than 10/microliter, and number of days with parasitemia higher than
136 10000/microliter (see Table S3).

137 As with Molineaux *et al.*, it tracks 50 different variant specific parasites, starts the infection
138 with only one variant expressed, tracks the parasites in 2-day time steps, and includes three
139 different types of immune responses. The model describes the total number of asexual
140 parasites via a flowchart which acts more like a decision tree with triggers different equations

141 for given parasite numbers (5) (see equations in the Table S2). At each time step the parasites
142 undergo replication with a multiplication rate of 16, and the probability of success of the
143 replication is computed from Binomial distribution dependent on the general adaptive and
144 variant specific immune response. Thus, in the absence of any immune response, the
145 parasites have a constant growth rate of 16.

146 The innate immune response in Gatton & Cheng is activated after reaching a threshold and is
147 assumed to increase with a higher number of parasites until a maximum effect is reached.
148 The effect of the variant specific immune response is modeled as being inversely proportional
149 to the number of antibodies produced, the latter being computed at each time step. The
150 magnitude of the antibody response is dependent on whether this antibody has previously
151 been produced during the infection, as well as cross-reactivity (so that an antibody response
152 against a specific variant also has a small effect on all other variants). The general adapted
153 immune response is only dependent on the time of infection, thus not changing with parasite
154 numbers, nor does it differ between individuals (see Table S2). Additional biological
155 differences between the model of Gatton *et al.* compared to Molineaux *et al.* and Johnston *et*
156 *al.* is the switching mechanism from one variant to another, which in Molineaux *et al.* and
157 Johnston *et al.* is assumed to depend on the variant specific immune response, whereas in
158 Gatton & Cheng it is completely independent from the host's immune response. In addition,
159 Gatton & Cheng assumes two populations of variants, either fast or slow switching, with 10
160 variants considered fast switching (rate ~ 0.5-4.5%) and 40 in the slow switching group (rate
161 ~ 9.10-11.8 %) , compared to 0.02% in Molineaux *et al.* and Johnston *et al.*. Switching
162 dynamics were previously investigated by the author (7) and based on *ex-vivo* analysis of var
163 gene transcripts of parasites isolated two volunteers who underwent challenge infection (8).

164 **Eckhoff (9)**: A summary and illustration of this model can be found on (10). This model has
165 both discrete and continuous components, to represent discrete events such as schizont
166 rupture in a two-day interval and the antibody response against merozoites, and to represent
167 the continuous immune components acting on infected red blood cells (iRBCs). This model is
168 more complex in the immune response mechanisms described, compared to the Molineaux *et*
169 *al.* and Molineaux adapted models, as it explicitly includes antibody responses to PfEMP1
170 and with smaller effect to minor epitopes, it includes immunological memory of the antibody
171 response, and it includes continuous and discrete immune responses.

The blood-stage immune response is divided into four components, namely the innate immune response, the antibody immune response against each PfEMP-1 variant, and each shared minor epitope, and the antibody immune response against merozoite proteins (such as MSP-1 and AMA-1). As for the Molineaux *et al.* and Molineaux adapted models, the innate immune response is assumed to limit the maximum parasite density (first peak). This innate immune response acts against both -iRBCs (continuous component) and against ruptured schizonts (discrete component). Its effect is activated by a pyrogenic threshold, and it decreases with increased antibody levels. The antibody response is dependent on the capacity to generate specific antibodies, which depends on the concentration of the variant specific parasite and on the immune memory to the parasite. Similarly, to other models, the antibody response decays once the corresponding parasite population is absent, but the antibody production capacity keeps an immunological memory. Thus, once exposed again to the same variant, the antibody response will reach higher levels faster. The immune response against merozoite proteins has a similar effect as the general adaptive immune response in the other models. It increases in time and leads to a decrease of the parasite peaks amplitude in time. The PfEMP1 variant specific immune response eventually clears the infection.

Initially, the model was fitted to malariatherapy data, but contrary to Molineaux *et al.,* the dataset includes patients with reinfection (as memory of immune response is modeled) and the perturbed ones to avoid selection biases. Parameters are either assumed through literature, or fitted to the malariatherapy dataset (details in (9)). The model outputs were compared to the first parasite density peak, lower secondary peaks, and lower peaks after 100 days, the possibility of reinfection with homologous strains, the interval between peaks, and the distribution of measured durations (9). The model has been re-fitted more recently using field data (11), and re-calibrated parameters included the number of PfEMP1 variants the switching rate, the number of MSP variants in the overall parasite population, the fraction of merozoites inhibited by maximum MSP1-specific antibody level, the number of minor epitope variants, and the kill rate of infected red blood cells due to antibody response to minor epitopes. As described in (11), a Dirichlet-multinomial distribution was used to compare simulation data with field data (12,13).

Childs & Buckee (14): This is a deterministic discrete model with 2-day time steps. It tracks parasite population of 60 variants and includes four different immune mechanisms. The immune response includes innate, variant specific, general adaptive immune response, similar

204 to the other models, as well as a cross-reactive immune response. Parasite growth depends on
205 the variant specific inherent multiplication rate, drawn from a Normal distribution, and
206 parasite growth is limited by red blood cell availability. Similar to the other models, the
207 innate immune response depends on the current number of parasites, the variant and cross-
208 reactive immune response depend on the variant specific (or group of variants for the cross-
209 reactive immune response) parasites, and the general immune response grows slowly during
210 the course of an infection. Differing to the other models, the four immune responses are all
211 capped by a maximum efficacy level, and the variant specific and cross-reactive immune
212 response depend on the number of available immune cells. The cross-reactive immune
213 response acts on groups of variants randomly grouped and pre-determined. The general
214 immune response, instead of being dependent on time or cumulative parasite density like the
215 other models, here increases each day that the number of parasites are above a certain
216 threshold.

217 Because the main aim of this model was to understand the key assumptions of the biological
218 mechanisms included in the mechanistic within host model, the model's main advantage
219 compared to the others rely on the sensitivity analysis in the parameter values. Indeed, it is a
220 deterministic model, but a wide range of values for all the parameters have been evaluated
221 using the Latin Hypercube Sampling method. In addition, different switching networks,
222 enabling parasites to switch from one variant to another, were evaluated.

223 **Gurarie *et al.* (15):** This is a discrete 2-day time step model. In this model there is a
224 continuous production and loss of uninfected RBCs, which can become infected by the
225 release of merozoites, and parasite replication is inhibited by two immune effectors, innate
226 and adaptive. The merozoite invasion depends on available RBCs so that when the ratio
227 between the number of merozoite and the number of available RBCs becomes large,
228 merozoites start competing for available RBCs. Despite this assumption, it is not clear RBC
229 availability is important for human *P. falciparum* infection. The innate immune response
230 depends on the number of infected cells, activated after reaching a certain parasite density
231 threshold level, and reaching a maximum clearance level. The adaptive immune response is
232 triggered by the product of infected RBCs, and the combined effector pool of the innate and
233 adaptive response, which is a way to allow for adaptive immune memory, and it also depends
234 on an activation threshold. Similar to the other models, the adaptive immune response takes
235 more time to develop but has a slower decay time compared to the innate immune response.

236 Rather than explicitly modelling the different variant populations, the variant switching
237 dynamics, and variant specific immune response, such as in other models, the model greatly
238 simplifies the equations by using proxies of the more complex underlying mechanisms. First
239 the model only includes innate and adaptive immune responses, making no distinction
240 between the variant specific and general adaptive immune response. Second the parasite
241 population is taken as a whole and does not differentiate between the variant-specific
242 populations. Nevertheless, the variant switching and resulting decrease in an effective
243 adaptive immune response is implicitly accounted for by forcing "random falls" at each
244 replication cycle (where potentially parasites switched to a new variant) of the effective
245 adaptive immune response. To implicitly account for the variant-transcending immune
246 response, the amplitude of the random falls of the effective adaptive immune response
247 decrease in time.

248 The model was fitted using the malariatherapy data (from 122 patients), and each
249 malariatherapy patient was considered a random realization of a stochastic process. The
250 fitting process was done in two steps to fit the first parasitemia peak assumed deterministic
251 and a second stochastic step for parasitemia post first peak. The model outcome was
252 compared to minimum and maximum of parasite density time-series for each patient, and 50
253 simulations per patient were selected as an ensemble of best choices (Table S3). The
254 calibration process of the model resulted in a range of parameter values that can be randomly
255 chosen at each realization, and thus allow for variability in the parasite dynamics as observed
256 in the malariatherapy dataset. These parameters relate to the invasion probability, the
257 replication of parasites, immune response efficiencies and activation thresholds, and the
258 assumed antigenically distinct variant clusters.

259 **McKenzie & Bossert (16) :** This model is the only model studied here that uses differential
260 equations rather than discrete equations to represent the malaria within host dynamics. The
261 model includes merozoite replication and conversion of parasites into gametocytes and
262 includes the effect of two types of immune responses, innate and adaptive. There is no
263 distinction of variant specific parasites. Both immune responses are stimulated by the asexual
264 density, with a stronger stimulus of the innate effectors, but the dynamic of the innate
265 effectors assume the decay and the removal of the effectors, while the adaptive immune
266 response grows with the asexual parasite density and has no decay or removal in time (note

267 that the equation for the adaptive effectors include a decay component, but its parameter w =
268 0 in (16).).

269 Although not explored in this study, the model tracks different genotypes, includes cross-
270 reactivity, and in addition, investigated several aspect of gametocyte dynamics. Cross-
271 reactivity is included by allowing for immune responses to one genotype to be stimulated by
272 the asexual parasite density of another genotype.

273 The model was fitted to data from 63 malariatherapy patients who were inoculated with the
274 McLendon strain, including only the parasite densities in time before any drug was
275 administered. The model was fitted to data from each of the 63 patients individually, using
276 the steepest-descent algorithm and comparing model outputs to parasite density time-series
277 (Table S3), and an average of the parameter values was reported and used for their
278 transmission model.

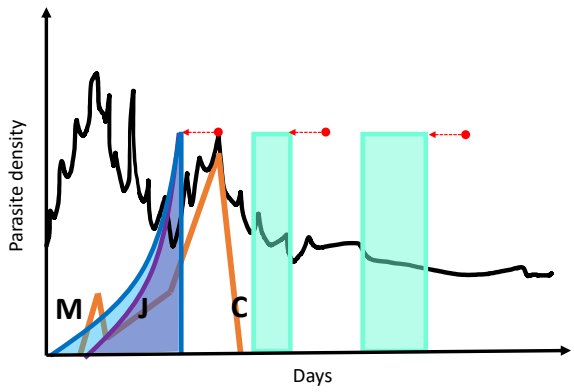

Figure S1: Schematic illustration of an infection and variant specific immune responses at a given time point from models Molineaux et al., Johnston et al., and Challenger et al.. *Example illustration of total parasite density in time (black) with an example of a single variant parasite density in orange. The parasite density affecting the variant specific immune response is represented by the coloured area in blue for Molineaux et al., in purple for Johnston et al., and in green for two examples at two different time points for Challenger et al.. At a given time point, represented by a red dot, the variant specific immune response in the Molineaux et al. (M) and Johnston et al. (J) model depend on the variant specific parasite density (orange) from eight days prior to the time point, and the effect of the parasite density decreases in time, with Molineaux et al. assuming a slower decay rate than Johnston et al.. For Challenger et al. (C), the total parasite density (black) in a given time frame eight days prior to the time point affect the variant specific immune response, with the time frame increasing further along in the infection, implicitly including immune memory, here represented by an example of two time points (red).*

Table S1 : Summary statistics of the observed malariatherapy data and the models*. Summary statistics from the simulation are shown in the first row, and the published results in the second row in italics. Source of published statistics: data [1], Johnston et al.(2), Challenger et al.(4), Gatton & Cheng (5).*

	Data			**Molineaux *et al***			**Johnston *et al***			**Challenger *et al***			**Gatton & *Cheng***			**Eckhoff**		
	med	min	max	med	min	max	med	min	max	med	min	max	med	min	max	med	min	max
initial slope	**0.49**	0.19	0.87	**0.50**	0.22	0.74	**0.52**	0.19	0.74	**0.49**	0.15	0.72	**0.47**	0.28	0.56	**0.35**	0.32	0.39
				0.49	*0.19*	*0.87*	***0.52***	*0.24*	*0.75*	***0.49***	*0.25*	*0.71*						
log10(density) peaks	**4.79**	3.37	5.66	**4.91**	4.46	5.30	**4.73**	3.55	5.58	**4.66**	3.49	5.56	**4.93**	4.49	5.54	**4.80**	4.76	4.84
				4.79	*3.37*	*5.66*	***4.78***	*3.69*	*5.67*	***4.77***	*3.57*	*5.61*	***4.81***	*4.47*	*5.31*			
n peaks	**10.00**	2.00	15.00	**5.83**	3.83	15.49	**9.19**	2.20	16.74	**7.31**	1.20	16.23	**5.86**	1.03	11.66	**6.71**	3.37	14.54
				10.00	*2.00*	*17.00*	***9.00***	*2.00*	*17.00*	***7.70***	*1.70*	*15.50*	***10.00***	*1.00*	*27.00*			
slope peaks	**-0.01**	-0.07	0.00	**-0.02**	-0.05	0.00	**-0.02**	-0.08	-0.01	**-0.02**	-0.07	0.00	**-0.01**	-0.03	0.01	**-0.04**	-0.07	-0.02
				-0.01	*-0.07*	*0.00*	***-0.02***	*-0.09*	*-0.01*	***-0.01***	*-0.03*	*0.00*	***-0.01***	*-0.03*	*-0.01*			
geo. mean peak interval	**20.48**	14.40	77.77	**16.47**	10.95	39.61	**22.40**	14.19	46.77	**22.41**	12.31	57.67	**20.89**	13.55	31.97	**23.56**	15.51	42.45
				20.00	*14.40*	*77.80*	***14.60***	*1.50*	*28.40*	***22.80***	*12.20*	*61.00*	***22.00***	*14.20*	*29.30*			
sd peak interval	**0.20**	0.03	0.47	**0.17**	0.03	0.50	**0.31**	0.10	0.57	**0.21**	0.05	0.38	**0.19**	0.03	0.29	**0.25**	0.08	0.35
				0.20	*0.03*	*0.47*	***0.31***	*0.04*	*0.56*	***0.22***	*0.03*	*0.48*	***0.22***	*0.07*	*0.29*			
prop. + 1st half	**0.88**	0.37	1.00	**0.86**	0.25	0.95	**1.00**	0.69	1.00	**1.00**	0.35	1.00	**0.90**	0.64	1.00	**0.75**	0.37	1
				0.88	*0.40*	*1.00*	***0.97***	*0.57*	*1.00*	***0.97***	*0.46*	*1.00*	***0.67***	*0.48*	*1.00*			
prop. + 2nd half	**0.45**	0.07	0.93	**0.33**	0.00	0.90	**0.66**	0.12	1.00	**0.99**	0.21	1.00	**0.75**	0.52	1.00	**0.28**	0.09	0.88
				0.46	*0.08*	*0.94*	***0.58***	*0.12*	*1.00*	***0.79***	*0.10*	*1.00*	***0.61***	*0.37*	*1.00*			
last + day	**215**	37	405	**142**	74	599	**182**	37	366	**123**	24	257	**129**	20	265	**177**	82	439
				215	*37*	*405*	***193***	*38*	*404*	***198***	*39*	*409*	***239***	*10*	*590*			

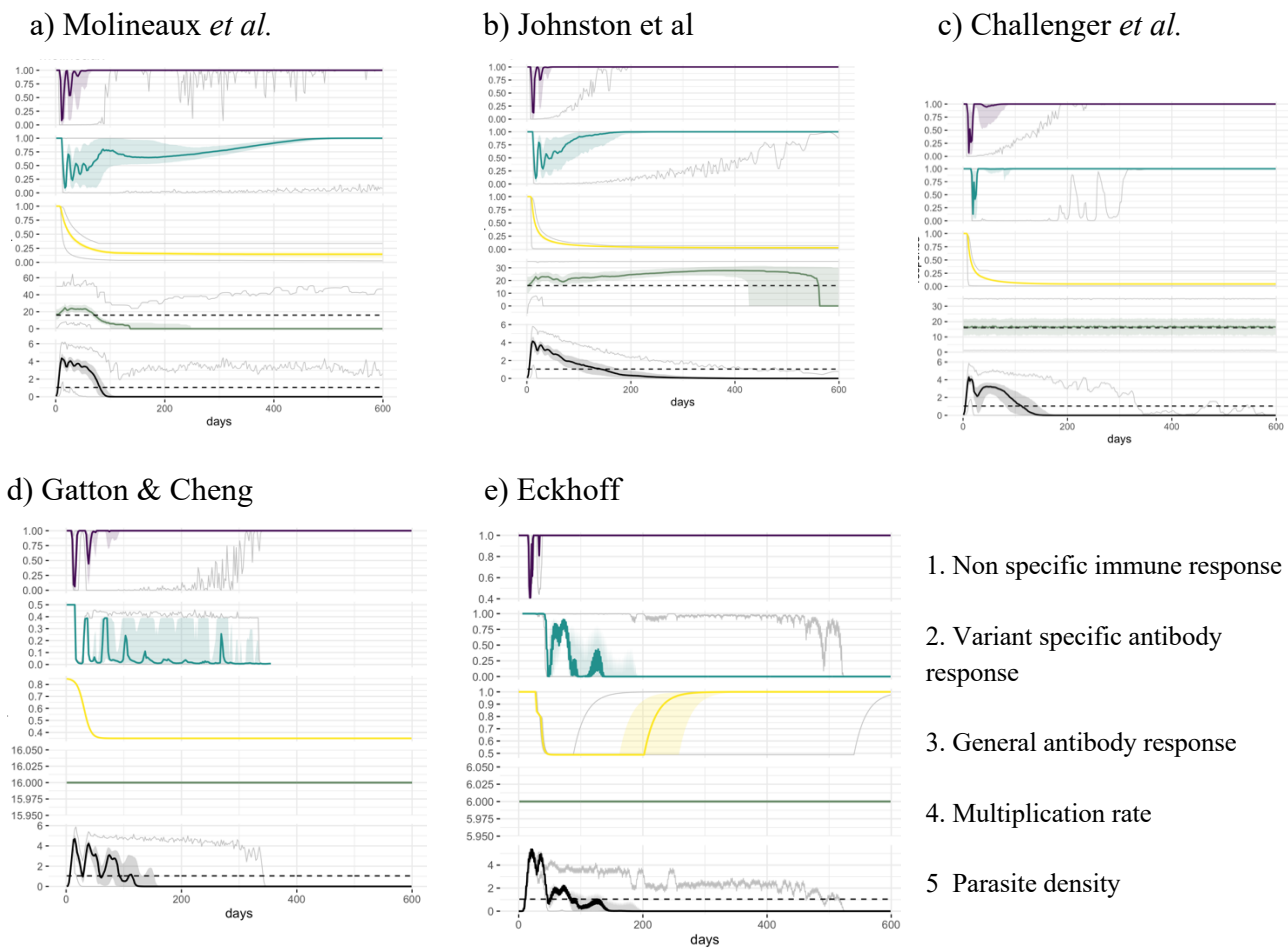

Figure S2: Immune responses, multiplication rates and asexual parasite densities in different models. *Each panel shows, from top to bottom, 1. the effect of the innate immune response, 2. the effect of the variant specific immune response (see methods for calculations), 3. the effect of the general adaptive immune response, 4. the net effect of the product of the three immune responses, 5. the average (across variants, see methods) multiplication rate, 6. the log10 asexual density and 7. the product of the average multiplication rate with the net effect of the immune response. X-axis represents days of infection, solid line the median, shaded area the interquartile range (Q25-Q75) and the gray lines the minimum and maximum resulting from the 1750 simulations. The horizontal dashed green line represents an average multiplication rate of 16, the horizontal dashed black line indicate the threshold of positive density (10PBRC/µl). Results are shown for* ***a)*** *Molineaux et al.,* ***b)*** *Johnston et al., and* ***c)*** *Challenger et al.,* ***d)*** *Gatton & Cheng, and* ***e)*** *Eckhoff*

Table S2: Model equations

Within-host mechanistic models		
Molineaux *et al. (1)* and *Molineaux adapted* models (2,4)	Gatton & Cheng model (5)	Eckhoff (9)
Parasite dynamics		
Parasite replication, influenced by immune responses, and antigenic variation • *Molineaux et al. and Johnston et al.* $P_i(t+2)' = \left((1-s)P_i(t) + sp_{i(t)}\sum_{j=1}^{v} P_j(t)\right) m_i S_c(t) S_i(t) S_m(t)$ • *Challenger et al.* $P(t+2) = m(t)S_c(t)S_v(t)S_m(t)P(t)$ *Parasite density* • *Molineaux et al. and Johnston et al.* $P_c(t) = \sum_{i=1}^{v} P_i(t)$ $P_i(t+2) = \begin{cases} P_i(t+2)' & if\ \ P_i(t+2)' \geq 10^{-5} \\ 0 & otherwise \end{cases}$	*Number of parasites* $X_t = \sum_{i=1}^{50} X_{t,i}$ $X_t = \begin{cases} X_t & if\ \ X_t \geq 1 \\ 0 & otherwise \end{cases}$ *Parasite antigenic variation* $X_{t,i} = X_{t,i} + st_{t,i} - sw_{t,i}$ Parasite replication, influenced by immune responses $X_{t+1,i} = \mathrm{Bi}(16X_{t,j}, (1-m_t)/Ab_{t,i})$ • If $X_t > NSI\ threshold\ (T)$: $X_{t,i} = \begin{cases} Bi\left(X_{t,i}, \exp\left(-k * \frac{X_t - T}{T}\right)\right)\ if\ k(X_t - T) \leq 10 \\ Bi\left(X_{t,i}, \exp(-10)\right)\ if\ k(X_t - T) > 10 \end{cases}$	$t_{asexual} = T_{asexual}$, and $t_{asexual,n+1} = t_{asexual,n} - \Delta t$ defines a 48h timer for including both continuous and discrete events. *Concentration per microliter of parasites expressing antigen i:* $X_i = N_i/(number\ of\ microliters\ of\ blood)$ *Number of IRBCs of antigen n created by previous generation expressing antigen n* $N_n^1 = \left((1 - k_{gametocyte})N_n - \sum^{nantigenswitch} N_{n+1,n}\right) N_{IRBCmerozoites} Z_{MS}$ *For all n, i=1 to* $n_{antigenswitch}$, *add in switching IRBCs* $N_{n+i}^1 = N_{n+i,n} N_{IRBCmerozoites} Z_{MS}$ *Number of IRBCs expressing antigen i whose merozoites will create IRBCs in the next generation n+1 expressing same antigen i* $N_{i,n+1} = N_{i,n} - Binomial(N_{i,n}, P_{kill,i})$ $P_{kill,i} = 1 - \exp\left(-\Delta t\left(\frac{C_{innate} Y_{fever}}{1 + Y_{fever}} + C_{antibody}\left(Y_{antibody,i} + Y_{Minorepitope,i} c_{MinorMod}\right)\right)\right)$
Antigenic switch		

• *Molineaux et al.and Johnston et al* $$p_i(t) = \begin{cases} 0 & if\ \ S_i(t) < 0.1 \\ \frac{q^i S_i(t)}{\sum_{j=1}^{v} q^j S_j(t)} & otherwise \end{cases}$$	$st_{t,i} = \sum_{\substack{j=1 \\ j\neq i}}^{50} Bi(X_{t,j}, 0.18\mathrm{p_i}/\sum_{i=1}^{50} p_i)$ $sw_{t,i} = \sum_{\substack{j=1 \\ j\neq i}}^{50} Bi(X_{t,i}, 0.18\mathrm{p_j}/\sum_{i=1}^{50} p_i)$ $$p_i = \begin{cases} 0\ for\ var\ 1 \\ 1\ for\ var\ 2 \\ \frac{p_{i-1}}{1.3}\ for\ var\ 3\ to\ c \\ \frac{p_{i-1}}{1*10^7}\ for\ var\ (c+1) \\ \frac{p_{i-1}}{1.18}\ for\ var\ (c+2)\ to\ 50 \end{cases}$$	*Number of IRBCs of antigen n switching to express antigen n+i* $$N_{n+i,n} = Poisson(K_{antigen}N_n), 1 \leq i \leq n_{antigenswitch}$$
Immune responses		
innate $$S_c(t) = \left(1 + \left(\frac{P_c(t)}{P_c^*}\right)^{\kappa_c}\right)^{-1}$$ *variant specific* • Molineaux *et al.*and Johnston *et al* $$S_i(t) = \left(1 + \left(\frac{\sum_{\tau=0}^{t-\delta_v} P_i(\tau) e^{-\sigma(t-\tau-\delta_v)}}{P_v^*}\right)^{\kappa_v}\right)^{-1}$$ • Challenger *et al* $$S_v(t) = \left(1 + \left(\frac{\sum_{\tau=f(t)}^{t-8} P(\tau)}{P_{v2}^*}\right)^{\kappa_v}\right)^{-1}$$	*innate* $$T = \begin{cases} 1/SF * 10^{0.271t+1.6864+N(0,0.3)}\ if\ t \leq 3 \\ 1/SF * 10^{3.39+N(0,0.3)}\ if\ t > 3 \end{cases}$$ *anti-PfEMP1* • If $X_{t,i} \geq 6 * 10^7$ for the first time in the last 20 days • Trigger antibody for variant *i* $$s_i = t + 4$$ $$A_i = \begin{cases} N(\alpha, 100) & for\ the\ first\ Ab\ produced \\ N(\alpha + 200, 100) & otherwise \end{cases}$$ $$B_i = N(\psi, 0.07)$$ • Calculate amount of antibody present for each variant	*innate* $$\begin{cases} for\ \ t_{asexual} > 0: \frac{dY_{innate}}{dt} = \frac{1}{\tau_{innate}} \frac{\sum_i X_i(1 - Y_{antibody,i})}{\sum_i X_i(1 - Y_{antibody,i}) + X_{50,innate}} \\ for\ t_{asexual} = 0: \Delta Y_{innate} = \frac{\sum X_{schizont}}{\sum X_{schizont} + X_{50,innate}} \end{cases}$$ $$Y_{fever} = k_{fever} Y_{innate}$$ *variant specific* For i=1 to 50, if $X_i > 0$ $$\frac{dY_{capacity,i}}{dt} = \begin{cases} \frac{k_{pfemporminor}}{\tau_{capacity}} \frac{X_i + k_{antibody,min} X_{50,antibody}}{X_i + X_{50,antibody}} (1 - Y_{capacity,i}), Y_{capacity,i} < 0.4 \\ \frac{1}{\tau_{hyperimmunity}} (1 - Y_{capacity,i}), Y_{capacity,i} \geq 0.4 \end{cases}$$ $$k_{pfemporminor} = \begin{cases} 1\ for\ PfEMP1 \\ k_{minormod}\ for\ minor\ epitopes \end{cases}$$

Variant transcending

$$S_m(t) = (1-\beta)\left(1+\left(\frac{\sum_{\tau=0}^{t-\delta_m}\hat{P}_c(\tau)e^{-\rho(t-\tau-\delta_m)}}{P_v^*}\right)^{\kappa_m}\right)^{-1} + \beta$$

$$\hat{P}_c(t) = \begin{cases} P_c(t) & if\ P_c(t) < C \\ C & otherwise \end{cases}$$

$$P_c^*(t) = k_c * (first\ local\ max.density)$$

$$P_m^*(t) = k_m * [(last\ pos.day) - (first\ pos.day)]$$

$$Ab_{t,i} = \begin{cases} A_i z_i e_i^{-Bz_i} & if\ t > s_i \\ 1\ if\ t \le s_i\ and\ Ab_{t,j} = 1\ for\ all\ j \\ 1.05\ if\ t \le s_i\ and\ Ab_{t,j} > 1\ for\ any\ j \end{cases}$$

$$z_i = (2t - s_i)/30$$

General adaptive

$$m_t = m_0 + 0.5/(1+\exp(-(2t-30)/6))$$

$$\frac{dY_{antibody,i}}{dt} = \frac{1}{\tau_{abprod}}\left(Y_{capacity,i} - Y_{antibody,i}\right), Y_{capacity,i} > 0.3$$

For i=1 to 50, if $X_i = 0$

$$\frac{dY_{capacity,i}}{dt} = -\frac{1}{\tau_{capdecay}}\left(Y_{capacity,i} - Y_{memory}\right), Y_{capacity,i} > Y_{memory}$$

$$\frac{dY_{antibody,i}}{dt} = -\frac{1}{\tau_{abdecay}}Y_{antibody,i}$$

Anti-MSP

$$if\ t_{asexual} = 0$$

$$\Delta Y_{MSP} = K_{MSP}\frac{\sum X_{schizont}}{\sum X_{schizont} + X_{50,antibody}}(1 - Y_{MSP})$$

$$Z_{MS} = \left(1 - C_{merozoite}Y_{antibody,MSP}\right)$$

Variables

$P_i(t)$ = density of variant *i,* as PRBC/µl blood

$P_c(t)$ = total parasite density, as PRBC/µl blood

- Molineaux *et al.* and Johnston *et al.*

$p_i(t)$ = probability that a switching PBRC switches to variant *i*

$S_c(t), S_i(t), S_m(t)$ = probability that a parasite of variant *i* escapes control by the innate immune response, acquired variant-specific immune response, and acquired variant-transcending immune response, respectively, in the interval (t,t+2)

$X_{t,i}$ = number of parasites of variant *i*

X_t = total number of parasites

$st_{t,i}$= number of parasites switching to variant *i*

$sw_{t,i}$= number of parasites switching from variant *i*

p_i = switch rate

T , $Ab_{t,i}$, m_t = innate immunity, anti-PfEMP1 antibodies ,clonal immunity

N_n = number of IRBCs expressing antigen n

$N_{n,n+i}$ = number of IRBCs expressing antigen n whose merozoites will create IRBC's in the next generation expressing antigen n+i

N_n^1 = number of IRBCs in the new asexual cycle expressing antigen i

X_i = Concentration per microliter of parasites expressing antigen i

Y_{innate} = Level of pro-inflammatory cytokines

Y_{fever} = Level of fever due to pro-inflammatory cytokines

• Challenger *et al* $S_c(t), S_v(t), S_m(t)$ = probability that a parasite escapes control by the innate immune response, acquired variant-specific immune response, and acquired variant-transcending immune response, respectively, in the interval (t,t+2)		$Y_{antibody,i}$ = Level of antibodies specific to antigen *i* $Y_{capacity,i}$ = Variable representing changing capacity to produce antibodies specific to antigen *i*
Parameters		
v = number of variants per clone s = fraction of parasites switching among variants per two-day q = parameter of the geometric distribution of switching probabilites P_c^*, P_m^* = two host-specific critical densities k_c, k_m = two constants allowing calculation of P_c^*, P_m^* from host specific data P_v^* = critical density of a variant, common to all variants $\kappa_c, \kappa_v, \kappa_m$ = stiffness parameters for a saturation of innate immune response, acquired variant-specific immune response, and acquired variant-transcending immune response C = maximum daily antigenic stimulus, per µl, of the acquired variant-transcending immune response σ = decay parameters, per day, of the acquired variant-specific immune response δ_v, δ_m = delay parameters, in days, of the acquired variant-specific and variant transcending immune response, respectively β = maximum value of S_m	Switching parameters: • c; number of 'fast' switching *var* genes Non specific immunity • SF, scaling factor correcting for difference between onset of NSI and pyrogenic threshold • k, feedback constant for sensitivity of parasites to NSI response Specific immunity • m_0 probability of parasites being killed by specific immunity at start of blood-stage infection Anti-PfEMP1 immunity • α, parameter influencing magnitude of antibody response • Ψ (months^{-1}), reciprocal of time to antibody peak	Immunological: $X_{50,innate}$ = parasitemia at which innate immune response is half of maximum $X_{50,capacity}$ = parasitemia at which antibody immune response is half of maximum τ_{innate} = inverse of maximum immune response rate $\tau_{capacity}$ = inverse of maximum antibody response rate $\tau_{hyperimmunity}$ = inverse of development of hyperimmunity $k_{antibodymin}$ = minimum antibody response to antigen $k_{minormod}$ = modification of response rate for minor epitopes C_{innate} = rate at which innate immune response kills IRBCs $C_{antibody}$ = rate at which specific antibody immune response kills IRBCs $C_{minormod}$ = modification of antibody kill rate for minor epitopes $C_{merozoite}$ = maximum blocking of merozoite invasion by MSP antibodies K_{MSP} = per cycle growth rate of MSP antibody response

$m_i \sim N(\mu_m, \sigma_m^2)$ *truncated to ensure* $m_i \geq 1$ (*Molineaux et al*) *or* $35 \geq m_i \geq 1$ (*Johnston et al*) : basic multiplication factor, per two-day cycle, of variant *i;* $m \sim N(\mu, \sigma), \frac{\langle (m(t)-\mu)(m(t-\theta)-\mu) \rangle}{\sigma^2} = g^{\theta}$, $0 < g < 1$: average growth rate at time t		Y_{memory} = immunological memory level $T_{hyperimmunity}$ = duration of hyperimmunity after removal of antigen Parasitological: $N_{IRBCmerozoites}$ = Merozoites per IRBC schizont $T_{asexual}$ = Duration of asexual cycle $N_{variants}$ = Number of PfEMP-1 variants per clone $N_{minorepitopes}$ = Number of minor epitopes per clone $K_{antigen}$ = PfEMP-1 switch rate $n_{antigenswitch}$ = number of non-suppressed available variants per IRBC
Comparing immune response effects between Molineaux *et al.*and *Molineaux adapted* models with Gatton *et al.*and Eckhoff		
• *effect of the innate immune response*		
S_c	$\exp\left(-\frac{k(X_t - T)}{T}\right)$	$\exp\left(-C_{innate}\frac{k_{fever}Y_{innate}}{1 + k_{fever}Y_{innate}}\right)$
• *effect of the variant specific immune response*		
$S_{v,i}$	$1/Ab_{t,i}$	$\exp\left(-C_{antibody}(Y_{antibody} + Y_{minorepitope}\, c_{MinorMod})\right)$
• *effect of the general adaptive immune response*		
S_m	*1-m(t)*	$Z_{MS} = (1 - C_{merozoite}\, Y_{antibody,MSP})$
Within-host mechanistic models		
Childs & Buckee (14)	Gurarie *et al (15)*	McKenzie & Bossert (16)
Parasite dynamics		

Number of parasites, dependent on growth and immune responses $P_i(t+1) = g_i(t+1)I(t+1)\Gamma_{VS_i}(t+1)\Gamma_{CR_i}(t+1)M(t+1),$ *Parasite growth, dependent on intrinsic growth rate and inherent switching between variants, limited by red blood cells availability* $g_i(t+1) = \left(1 - \exp\left(-\frac{K(t)}{\sum_j p_j(t)}\right)\right)\left[\gamma_i p_i(t)(1-\omega_i) + \omega_i \sum_{j \neq i} \gamma_j \beta_{ji} p_j(t)\right]$	*Uninfected red blood cells, depend on homeostatic production and loss of red blood cells, and the loss due to merozoite invasion* $x' = (1-\delta)x_0 + \delta x - \rho\left(\frac{M}{x}\right)x$ *Infected red blood cells, depend on combined level of innate and adaptive immune response, and on merozoite invasion* $y' = 2^{-(a+b)}\rho\left(\frac{M}{x}\right)x$ *Merozoite equation depends on the effective replication rate of the parasite:* $M = ry + S$ *Effective probability of invasion decreases according to:* $\rho(z) = 1 - e^{-z}$ $z = M/x$	*Asexual parasite density, depend on daily replication of asexual parasite, daily conversion into gametocytes, and the effect of immune response:* $\frac{dM_u}{dt} = (a_u - z_u - c_u I - \Sigma b_{u,v} J_v)M_u$
Antigenic switch		
$g_i(t+1) \propto \omega_i \sum_{j \neq i} \gamma_j \beta_{ji} p_j(t)$	-	-
Immune responses		
innate $I(t+1) = \min\left(E_I, \left(\frac{1+\sum_i p_i(t)}{1+\sum_i p_i(t) + C_I}\right)E_I\right)$ *variant specific* • *Dynamics of immune cells, depend on pre-existing cells, expansion when variant specific parasites in large quantities, decay, and restricted by total number of immune cells available*	*Innate effectors, stimulation triggered by parasite level relative to threshold A, and has a short life span* $a' = f_a \phi_a\left(\frac{y}{A}\right) + \sigma_a a$ *Adaptive effectors, stimulation triggered by parasite level relative to threshold B, and has a longer life span* $b' = q f_b \phi_b\left(\frac{y(a+b)}{B}\right) + \sigma_b b$	*innate immune effectors* $\frac{dI}{dt} = \Sigma s_v M_v - I\Sigma k_v M_v - qI$ *acquired immune effectors:* $\frac{dJ_u}{dt} = \Sigma r_{u,v} M_v - w_u J_u$

$$VS_i(t+1) = VS_i(t)\left(1+\pi_{VS}\exp\left(-\frac{\psi_{VS}}{p_i(t-\tau)+1}\right)\right)\left(1-\mu_{VS}\left(1-\exp\left(-\frac{\psi_{VS}}{p_i(t)+1}\right)\right)\right)\left(1-\exp\left(-\frac{K_{Imm}}{\sum_j VS_j(t)}\right)\right)$$ • *Effectiveness of response, depend on relative amount of parasite variants and specific immune cells* $$\Gamma_{VS_i}(t+1) = E_{VS}\left(1-\exp\left(-\frac{1+g_i(t)}{VS_i(t)}\right)\right)$$ *cross-reactive:* • *Dynamics of immune cells, depend on pre-existing cells, expansion when group of variant specific parasites in large quantities, decay, and restricted by total number of immune cells available* $$CR_i(t+1) = CR_i(t)\left(1+\pi_{CR}\exp\left(-\frac{\psi_{CR}}{1+\sum_{j\sim i}p_i(t-\tau)}\right)\right)\left(1-\mu_{CR}\left(1-\exp\left(-\frac{\psi_{CR}}{1+\sum_{j\sim i}p_i(t)}\right)\right)\right)\left(1-\exp\left(-\frac{K_{Imm}}{\sum_j CR_j(t)}\right)\right)$$ • *Effectiveness of response, depend on relative amount of a group of parasite variants and specific immune cells* $$\Gamma_{CR_i}(t+1) = E_{CR}\left(1-\exp\left(-\frac{1+\sum_{j\sim i}g_i(t)}{CR_i(t)}\right)\right)$$ *Variant transcending*	• *Antigenic variation accounted for by random falls in effector, q_0^t an exponential function with base:* $$q_0 = 2^{-1/m} < 1$$	

$M(t+1) = \min\left(E_M, \frac{1+\sum_t \chi_t}{1+C_M+\sum_t \chi_t} E_M\right)$ $\chi_t = \begin{cases} 1, & if \ \sum_i p_i(t) > 10^7 \\ 0 & otherwise \end{cases}$		
Variables		
$P_i(t)$ = overall number of parasites of the *i*th antigenic variant $g_1(t)$ = parasite growth, in the absence of any immune response $I(t), \Gamma_{VS_i}, \Gamma_{CR_i}, M(t)$ = effectiveness of the innate, variant specific, cross-reactive, and general immune response, respectively CR_i, VS_i= dynamics of the variant specific, and cross-reactive immune cells, respectively.	*x* = uninfected RBC measured per microliter of blood *y* = infected RBC measured per microliter of blood *M* = number of merozoites released (a result of y(t)) *a,b* = dimensionless variables representing innate and adaptive immune effectors, respectively	*M* = asexual forms *J* = acquired-immunity effectors *I* = innate-immunity effectors subscript *v* : different genotypes
Parameters		
Immunological: E_I, E_{VS}, E_{CR}, E_M = maximum efficacy of innate, variant specific, cross-reactive, and general immune response, respectively $C_I, \psi_{VS}, \psi_{CR}, C_M$ = half-maximal activation of innate, variant specific, cross-reactive, and general immune response, respectively $K(0), K_{Imm}$= restriction of total number of red blood cells, and immune cells, respectively μ_{VS}, μ_{CR} = maximum decay rate of variant-specific, and cross-reactive immune cells, respectively π_{VS}, π_{CR} = maximum growth rate of variant-specific, and cross-reactive immune cells, respectively	Immunological: *A,B* = Threshold to trigger innate and adaptive immune effectors, respectively ϕ_a, ϕ_b= Hill function defining innate and adaptive immune stimulation, respectively f_a, f_b= maximal stimulation efficiency of innate and adaptive immune response, respectively $a_M = \frac{f_a}{1-\sigma_a}$, $b_M = \frac{f_b}{1-\sigma_b}$ = maximal clearance levels of innate and adaptive immune effectors, respectively. $a_M + b_M \gg \log(r)$ δ_a, δ_b = survival rate per cycle of innate and adaptive effectors, respectively	Immunological: *c, b* = daily removal rate of asexual forms by innate-immune, and acquired immune response effectors, respectively *s, r* = rate of stimulation of the innate immune, and acquired immune response (effectors per asexual form) *k* = removal rate of innate-immune effectors (effectors per effector asexual form) *q, w* = decay rate of innate-immune, and acquired immune response effectors, respectively Parasitological: *a* = daily replication rate of asexual blood forms,

τ = delay of adaptive immune response activation (days) Parasitological: γ_i = intrinsic growth rate of variant *i* ω_i = percentage switching to a new variant from variant *i* β_{ji} = switching probability from variant *i* to variant *j*	Parasitological: *r* = effective replication rate *p* = probability of a merozoite to invade an uninfected RBC *m* = number of antigenically distinct variant clusters x_0 = normal concentration of uninfected RBC	*z* = conversion rate of asexual forms to gametocytes

Table S2: Model fitting, *as described in the initial publications. Fitting methods and data might have been modified subsequently.*

Models	**Molineaux *et al.***	**Johnston *et al.***	**Challenger *et al.***	**Gatton *et al.***	**Childs & Buckee.**	**Eckhoff**	**McKenzie & Bossert**	**Gurarie *et al.***
Fitting method	Informed trial and error (no systematic fitting) to find the best set of parameters. In a second step each patient was simulated 50 times (with different multiplication factors), and χ^2 was used to identify best patient specific match	Bootstrapping, not all parameter space explored. The model was run 1,000 times and 50 samples of 50 runs each were selected. Goodness-of-fit, was assessed with relative errors between model outputs tested outcome	Same than Johnston *et al*, but with MCMC using Metropolis-Hasting algorithm to generate random walks in parameter space	Fitted to the patient data using sets of 100 simulations, altering the 6 parameters until the distribution of simulations did not differ significantly to that of the patient data.	Stochastic sampling of parameters using a Latin Hypercube Sampling. Results include a minimum of 100 000 replicates. This model was not fitted but the range of parameter values were defined according to literature	Extensive simulations and ensembles of simulated infection trajectories generated for ranges of combinations consistent with observed infection behaviors.	Fitted the model to each of the 63 individual charts using a steepest-descent algorithm to determine the parameter set that minimized the sum of squared deviations. Starting values based on the literature and their previous work.	Two steps: a deterministic fit to the first wave of parasitemia, and a second stochastic step for parasitemia patterns following the initial wave. Based on these steps 'best choices' of in-host parameters are selected, by defining min/max ensemble envelop' by minimizing its

								distance from the ensemble mean curve
Outcome tested for the fitting	distribution of durations of infection from malariatherapy as well as the minimum, median, and maximum of the 9 summary statistics			max parasitemia, number of days with fever, number of days with parasitemia higher than 10 per microliter, number of days with parasitemia higher than 10000 per microliter		first parasite density peak, lower secondary peaks, and even lower peaks after 100 days, the possibility of reinfection with homologous strains, the interval between peaks, and the distribution of measured durations.	asexual parasite density and gametocyte parasite density over time for each patient chart	asexual parasite density over time for each patient chart
Fitted parameters	$q, k_c, k_m, P_v^*, \kappa_c, \kappa_v, \kappa_m$ $C, \sigma, \delta_v, \delta_m, \beta$	$\kappa_c, \sigma, P_c^*, P_m^*$	$\sigma, g, P_v^*, \kappa_m, f(t)$	$c, SF, k, m_0, \alpha, \Psi$	All parameter values are explored within ranges	Ranges of several parameters ($X_{50,innate}$, C_{innate}, $C_{antibody}$, $C_{minormod}$, $C_{merozoite}$, K_{MSP}, Y_{memory}, $K_{antigen}$) are investigated	a-z, zy, p, s, c, k, q, b, r	A, B, p, f_a, f_b, m

References

1. Molineaux L, Diebner HH, Eichner M, Collins WE, Jeffery GM, Dietz K. *Plasmodium falciparum* parasitaemia described by a new mathematical model. Parasitology. 2001 Apr;122(4):379–91.

2. Johnston GL, Smith DL, Fidock DA. Malaria's Missing Number: Calculating the Human Component of R0 by a Within-Host Mechanistic Model of Plasmodium falciparum Infection and Transmission. Antia R, editor. PLoS Comput Biol. 2013 Apr 18;9(4):e1003025.

3. Sama W, Dietz K, Smith T. Distribution of survival times of deliberate Plasmodium falciparum infections in tertiary syphilis patients. Trans R Soc Trop Med Hyg. 2006 Sep;100(9):811–6.

4. Challenger JD, Bruxvoort K, Ghani AC, Okell LC. Assessing the impact of imperfect adherence to artemether-lumefantrine on malaria treatment outcomes using within-host modelling. Nat Commun. 2017 Dec;8(1):1373.

5. Gatton ML, Cheng Q. Investigating antigenic variation and other parasitehost interactions in Plasmodium falciparum infections in nave hosts. Parasitology. 2004 Apr;128(4):367–76.

6. Paget-Mcnicol S, Gatton M, Hastings I, Saul A. The *Plasmodium falciparum var* gene switching rate, switching mechanism and patterns of parasite recrudescence described by mathematical modelling. Parasitology. 2002 Mar;124(3):225–35.

7. Gatton ML, Peters JM, Fowler EV, Cheng Q. Switching rates of Plasmodium falciparum var genes: faster than we thought? Trends Parasitol. 2003 May;19(5):202–8.

8. Peters J, Fowler E, Gatton M, Chen N, Saul A, Cheng Q. High diversity and rapid changeover of expressed var genes during the acute phase of Plasmodium falciparum infections in human volunteers. Proc Natl Acad Sci. 2002 Aug 6;99(16):10689–94.

9. Eckhoff P. P. falciparum Infection Durations and Infectiousness Are Shaped by Antigenic Variation and Innate and Adaptive Host Immunity in a Mathematical Model. Snounou G, editor. PLoS ONE. 2012 Sep 19;7(9):e44950.

10. Malaria infection and immune model — Malaria Model documentation [Internet]. [cited 2020 Nov 2]. Available from: https://docs.idmod.org/projects/emod-malaria/en/latest/malaria-model-infection-immunity.html

11. Selvaraj P, Wenger EA, Gerardin J. Seasonality and heterogeneity of malaria transmission determine success of interventions in high-endemic settings: a modeling study. BMC Infect Dis. 2018 Aug 22;18(1):413.

12. Gerardin J, Ouédraogo AL, McCarthy KA, Eckhoff PA, Wenger EA. Characterization of the infectious reservoir of malaria with an agent-based

model calibrated to age-stratified parasite densities and infectiousness. Malar J. 2015 Jun 3;14(1):231.

13. McCarthy KA, Wenger EA, Huynh GH, Eckhoff PA. Calibration of an intrahost malaria model and parameter ensemble evaluation of a pre-erythrocytic vaccine. Malar J. 2015 Jan 7;14(1):6.

14. Childs LM, Buckee CO. Dissecting the determinants of malaria chronicity: why within-host models struggle to reproduce infection dynamics. J R Soc Interface. 2015 Mar;12(104):20141379.

15. Gurarie D, Karl S, Zimmerman PA, King CH, St. Pierre TG, Davis TME. Mathematical Modeling of Malaria Infection with Innate and Adaptive Immunity in Individuals and Agent-Based Communities. Paul RE, editor. PLoS ONE. 2012 Mar 28;7(3):e34040.

16. McKenzie FE, Bossert WH. An integrated model of Plasmodium falciparum dynamics. J Theor Biol. 2005 Feb;232(3):411–26.